

2025

# Structural and biophysical characterization of hereditary gelsolin amyloidosis variants: Y447H and R454C

---

<https://hdl.handle.net/2144/52262>

*"Downloaded from OpenBU. Boston University's institutional repository."*

BOSTON UNIVERSITY

ARAM V. CHOBANIAN & EDWARD AVEDISIAN SCHOOL OF MEDICINE

Thesis

**STRUCTURAL AND BIOPHYSICAL CHARACTERIZATION OF  
HEREDITARY GELSOLIN AMYLOIDOSIS VARIANTS: Y447H AND R454C**

by

**WILLIAM B. EASON**

B.S., Plymouth State University, 2022

Submitted in partial fulfillment of the

requirements for the degree of

Master of Science

2025

© 2025 by  
WILLIAM B. EASON  
All rights reserved

Approved by

First Reader

---

Gareth Morgan, Ph.D.  
Research Assistant Professor, Medicine

Second Reader

---

Keith Tornheim, Ph.D.  
Associate Professor, Biochemistry & Cell Biology

## **DEDICATION**

This work is dedicated to my mother and father, Roberta and William Eason, and my late grandparents, Ronald and Norma Nickerson.

## **ACKNOWLEDGMENTS**

I express my gratitude to my first and second readers, Dr. Morgan and Dr. Tornheim, for reviewing my thesis and providing valuable feedback. I also thank the Boston University Amyloidosis Center, particularly for their guidance and provision of essential materials that sustained my project. Finally, I am grateful to my tutors, Ava and Monae, for their dedicated time and support in keeping me on track throughout the program.

**STRUCTURAL AND BIOPHYSICAL CHARACTERIZATION OF  
HEREDITARY GELSOLIN AMYLOIDOSIS VARIANTS: Y447H AND R454C**

**WILLIAM B. EASON**

**ABSTRACT**

Gelsolin (*GSN*), an actin-binding protein, undergoes alternative splicing to produce cytoplasmic and secreted plasma isoforms. In hereditary gelsolin amyloidosis (HGA), the D187N mutation in G2 impairs calcium binding, destabilizing the plasma isoform and enhancing furin cleavage to generate C68 fragments (68 kDa) that deposit systemically. This study explores the structural basis of gelsolin amyloidosis by examining full-length *GSN* and isolated G4 from wild-type and G4 mutants Y447H and R454C for stability and misfolding potential. Full-length and G4 *GSN* variants were recombinantly expressed, then evaluated for proteolysis via SDS-PAGE/Western blot and stability via far-UV CD spectroscopy, probing EDTA/Ca<sup>2+</sup>-dependent G4 differences.

Circular dichroism (CD) spectroscopy revealed predominant  $\alpha$ -helical content in G4, with melting temperatures ( $T_m$ ) shifting from 69°C (WT, EDTA) to 81°C (Ca<sup>2+</sup>), 67°C to 85°C (Y447H), and 84°C to 78°C (R454C), indicating Ca<sup>2+</sup>-dependent stabilization. Proteolysis assays showed WT degraded rapidly, while Y447H resisted and R454C formed stable dimers, suggesting disulfide-mediated resilience. Notably, no C68 fragments were detected in supernatant up to 24 hours, contrasting with HGA's G2-driven pathology.

These findings suggest G4 mutations enhance *GSN* stability, shifting its energy landscape away from amyloidogenic pathways. Y447H's Ca<sup>2+</sup>-bolstered fold and R454C's oligomerization highlight variant-specific mechanisms that may mitigate misfolding, offering insights into *GSN*'s structural regulation and potential therapeutic targets for HGA.

## TABLE OF CONTENTS

DEDICATION .....	iv
ACKNOWLEDGMENTS .....	v
ABSTRACT.....	vi
TABLE OF CONTENTS.....	viii
LIST OF TABLES .....	x
LIST OF FIGURES .....	xi
LIST OF ABBREVIATIONS.....	xiii
INTRODUCTION .....	1
Protein Folding and Disease .....	1
General Amyloidosis History .....	6
History of Hereditary Gelsolin Amyloidosis .....	7
Gelsolin Function.....	9
Genetics .....	12
Biochemistry.....	13
Clinical observations.....	17
Variants.....	21
Goal of Research.....	22
METHODS .....	23
RESULTS .....	30
DISCUSSION .....	39
REFERENCES .....	46

CIRRICUMLUM VITAE..... 52

## LIST OF TABLES

Table 1. Media. ....	26
----------------------	----

## LIST OF FIGURES

Figure 1. Schematic diagram of normal protein folding and alternative-pathway aggregate .....	3
Figure 2. Schematic representation of mutation of HGA leading to gain-of-toxic function effects .....	4
Figure 3. Representation of Autosomal Dominance in HGA .....	9
Figure 4. Structure of Gelsolin.....	11
Figure 5. Model of Gelsolin contribution to actin filament severing .....	12
Figure 6. Protein structure of Human GSN .....	15
Figure 7. Close-up of mutation D187N .....	16
Figure 8. Schematic representation of aberrant proteolysis of plasma GSN.....	17
Figure 9. Patient with various clinical manifestations relating to HGA .....	19
Figure 10. Histological analysis of fat tissue of patient with HGA .....	19
Figure 11A. Western blot analysis confirming the successful expression for constructed Wild type (WT) GSN and variants- Y447H (YH) and R454C (RC) .....	31
Figure 11B. Densitometric analysis of WT and variant GSN protein expression in supernatant collected 4 hours post-transfection from a 24-well plate .....	32
Figure 12A. Time-course analysis of 68 kDa fragment expression in WT and variant GSN proteins at 4-, 8-, and 24-hours post-transfection .....	34
Figure 12B. Densitometric analysis of full-length protein GSN expression in WT and variant proteins at 4-, 8-, and 24-hours post-transfection .....	35

Figure 13A. Proteolysis analysis of full-length WT and variant GSN proteins over seven time points.....	37
Figure 13B. Time course analysis of limited proteolysis for WT and variant GSN proteins (Y447H and R454C).....	38
Figure 14. CD spectra of recombinant GSN WT, Y447H and R454C proteins.....	41
Figure 15. Thermal stabilities of recombinant GSN wild-type and variant proteins, with N-terminal MKH 6 tags, assessed using CD spectroscopy.....	42
Figure 16. Gelsolin Domain 4 Limited Proteolysis with Proteinase K.....	43

## LIST OF ABBREVIATIONS

°C.....	Celsius
µM.....	Microgram
µL.....	Microliter
µM.....	Micromolar
A.....	Adenine
a.a.....	Amino Acid
AD.....	Alzheimer's disease
Amp.....	Ampicillin
Arg/R.....	Arginine
Asn/N.....	Asparagine
Asp/D.....	Aspartate
CTS.....	Carpal Tunnel Syndrome
CD.....	Circular Dichroism
CFTR.....	Cystic fibrosis transmembrane regulator protein
C.....	Cytosine
Cys/C.....	Cystine
DMEM.....	Dulbelcco's modification of eagle's medium
DNA.....	Deoxyribose nucleic acid
<i>E coli.</i> .....	<i>Escherichia coli</i>
EDTA.....	Ethylenediaminetetraacetic acid

FAP.....	Familial amyloidotic polyneuropathy
FBS.....	Fetal bovine serum
Gs.....	grams
<i>GSN</i> .....	Gelsolin gene
GSN.....	Gelsolin protein
$\Delta G$ .....	Gibbs free energy
G.....	Guanine
$\Delta H$ .....	Enthalpy
h.....	Hour
hrs.....	Hours
HGA.....	Hereditary gelsolin amyloidosis
H.....	Histidine
HEK293A.....	Human embryonic kidney 293 adherent cells
IMAC.....	Immobilized metal ion affinity column
IPTG.....	Isopropyl $\beta$ -D-1-thiogalactopyranoside
K.....	Kelvin
K.....	Lysine
kDa.....	Kilodalton
L.....	Liter
LCD2.....	Lattice corneal dystrophy type II
M.....	Methionine
min.....	Minute

mL.....	Milliliter
mm.....	Millimeter
nm.....	Nanometer
Ni-NTA.....	Nickel nitrilotriacetic acid
OD.....	Optimal density
PBS.....	Phosphate based saline
PCR.....	Polymerase chain reaction
PD.....	Parkinson's disease
PIP2.....	Phosphatidylinositol 4,5-bisphosphate
PMSF.....	Phenylmethylsulfonyl fluoride
rpm.....	Revolution per minute
$\Delta S$ .....	Entropy
SDS-PAGE.....	Sodium Dodecyl Sulfate-Polyacrylamide Gel Electrophoresis
SNP.....	Single nucleotide polymorphism
TBST.....	Tris-buffered saline with Tween 20
T.....	Thymine
$T_m$ .....	Melting point
WT.....	Wild type
Y.....	Tyrosine

# INTRODUCTION

## Protein Misfolding and Disease

Proteins are among the most diverse macromolecules with the mammalian cell proteome containing ~20,000 different protein coding genes, expanding to ~100,000–200,000 isoforms via alternative splicing and potentially over 1 million species with post-translational modifications (Venter et al., 2001; Kim et al., 2014; Wilhelm et al., 2014; GENCODE, 2025). Proteome integrity and cellular health are maintained by keeping parameters within homeostatic conditions, which include the synthesis, folding, and degradation of proteins (Hartl, 2017). The linear amino acid sequence carries the information needed to specify how a protein will fold and eventually lead to its biological function (Anfinsen, 1973). The polypeptide chain, even if it is small as ~100 amino acids can adopt several conformations as large as  $10^{30}$  (Hartl, 2017).

The biologically native state of many proteins is a functional, three-dimensional structure that is thermodynamically stable, though only slightly stable under physiological conditions (Atkins & de Paula, 2014). In thermodynamics, a structure is considered “favorable” if it has a lower free energy (Gibbs free energy  $\Delta G$ ) than the unfolded conformation, which reflects a balanced relationship between enthalpy ( $\Delta H$ )-the heat absorbed or released through molecular interactions such as hydrogen bonds, hydrophobic effects, and van der Waals forces-and entropy ( $\Delta S$ ), the measure of disorder (Atkins & de Paula, 2014). This can be described by the equation  $\Delta G = \Delta H - T\Delta S$ , where  $T$  is the absolute temperature in kelvin (K). When  $\Delta H < 0$  (exothermic), energy is

released as the protein folds into its compact native state, favoring spontaneity.

Alternatively, when  $\Delta H > 0$  (endothermic), energy is absorbed, thwarting spontaneity. If  $\Delta S > 0$ , disorder increases and favors the unfolded state; if  $\Delta S < 0$ , disorder decreases as the protein adopts its ordered native conformation, and disfavors spontaneity (Dill & Bromberg, 2010).

Protein folding becomes a delicate process and is prone to error due to its small  $\Delta G$  margin. Environmental stressors and kinetic traps—such as pH shifts or temperature changes—can lead to protein misfolding by disrupting pathways, resulting in non-native states or aggregates, like amyloid fibrils seen in Alzheimer's Disease (AD) (Dobson, 2003). To correct these errors, chaperone proteins often assist by stabilizing intermediates; however, if protein misfolding persists it can lead to toxic aggregates and loss-of-function (Hartl, 2011).

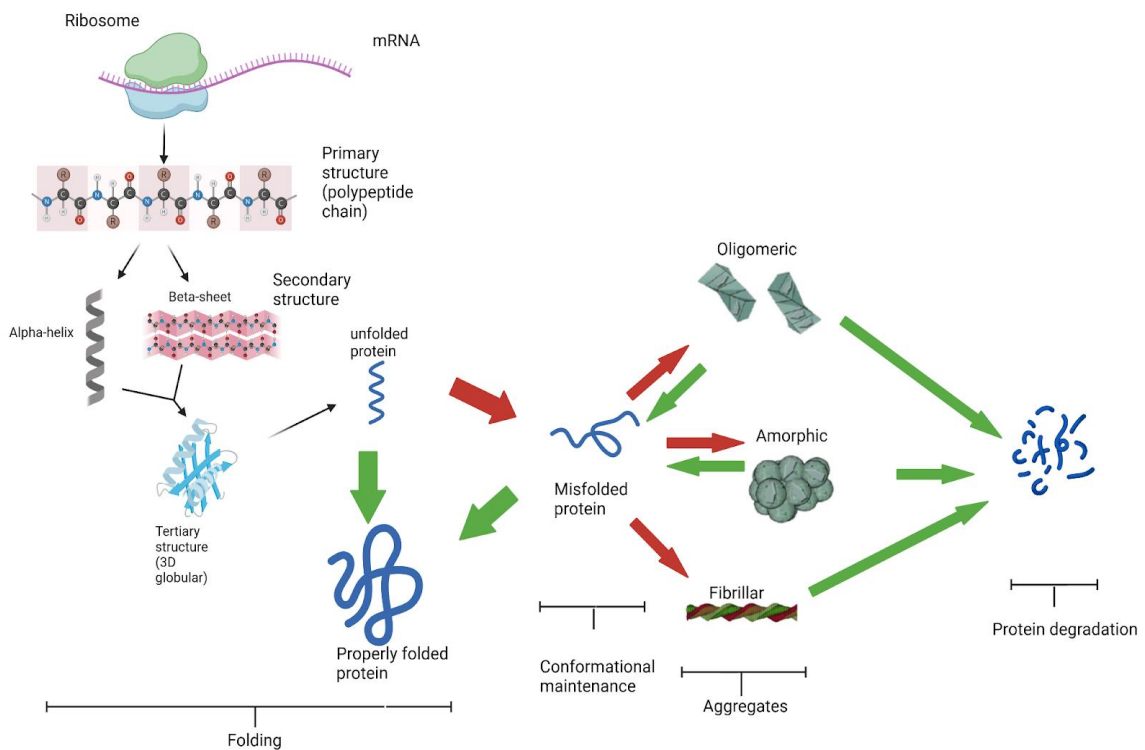


**Figure 1. Schematic diagram of normal protein folding and alternative-pathway aggregates.** Green arrows indicate assistance w/ chaperones; Red arrows indicate off-pathway interactions/intermediates.

Aberrant protein folding has been linked to a range of pathologies and has been characterized into two groups: loss-of-function and toxic gain-of-function (Hartl, 2017). Both groups can be caused by mutations including single nucleotide polymorphisms (SNP), insertions, and deletions. Loss-of-function mutations cause altered gene products that lack the molecular function of the wild-type gene, as in the case of cystic fibrosis transmembrane regulator protein (CFTR;  $\Delta F508$ ) (Riordan et al. 1989; Hartl, 2017).

Toxic gain-of-function mutations lead to metastable proteins that undergo aggregation in a process linked to cellular toxicity, which include diseases like AD, Parkinson's disease (PD), and Hereditary Gelsolin Amyloidosis (HGA) (**Figure 2**) (Solomon et al.2012; Hartl, 2017). In these cases, pathology is not necessarily linked to loss of normal protein function.

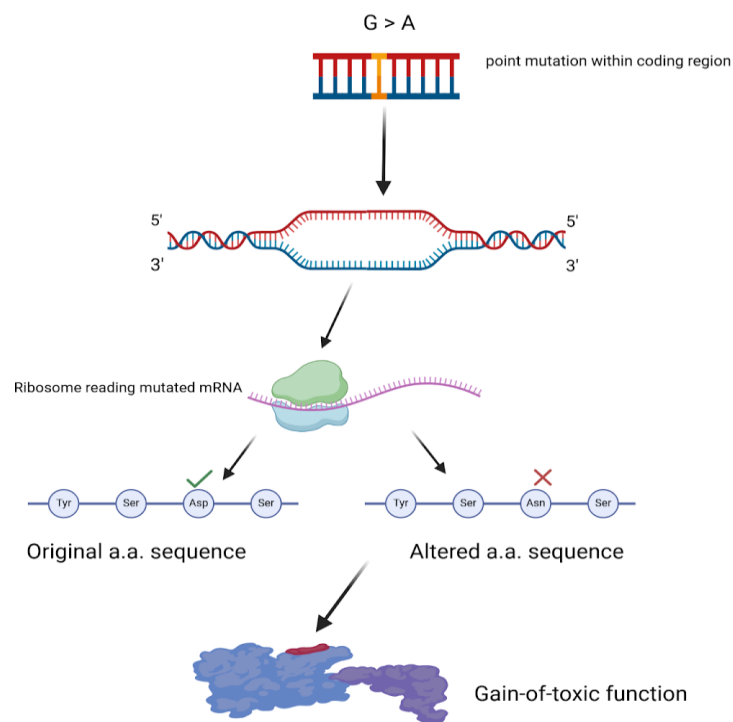


**Figure 2. Schematic representation of mutation of HGA leading to gain-of-toxic function effects.**

During proper folding hydrophobic forces operating within the molecule will stabilize its compact core (Solomon et al. 2012). Exposed hydrophobic residues, like valine and leucine, are thermodynamically unstable in an aqueous environment because of the hydrogen bonding network of adjacent water molecules, increasing solvent entropy costs (Tanford, 1980). In response, misfolded proteins will interact and bury these hydrophobic patches via protein-protein interfaces.  $\beta$ -structure becomes effective at making this possible. In this structure polypeptide strands will align side-by-side, enabling hydrophobic residues on nearby strands to pack closer together and away from water, as opposed to  $\alpha$ -helices, which fold individually and not known to promote intermolecular interactions (Chiti & Dobson, 2006). In a misfolded protein, the unstructured backbone—with its exposed peptide bonds—can form hydrogen bonds (Fändrich et al., 2001). Unlike  $\alpha$ -helices, where hydrogen bonds form intramolecularly within a single chain, the NH and C=O groups of  $\beta$ -sheet backbones hydrogen-bond with adjacent strands, forming an extensive network that can enhance stability depending on context.  $\beta$ -sheets form intermolecularly between separate proteins, making it ideal for aggregation and “zip up” misfolded proteins into a cohesive structure (Fändrich et al., 2001).

Misfolding is dependent on a protein’s energy landscape, where mutations, environmental conditions, and kinetic barriers can trap it in non-native states—often thermodynamically stable or kinetically persistent—different from its functional confirmation (Dill & Chan, 1997). The native state typically holds a composition  $\alpha$ -helices and  $\beta$ -sheets, but becomes inaccessible due to a high  $\Delta G$ , whereas the  $\beta$ -sheets

aggregates represent a deeper energy minimum for misfolded states (Dill & Bromberg, 2010).

### **General Amyloidosis History**

Amyloidosis is a group of diseases that are split into localized or systemic diseases (Bustamante & Zaidi, 2023; Buxbaum et al. 2024). These ailments are referred to as amyloid diseases due to the cross- $\beta$ -sheet aggregates or amyloid structures found within or outside the cells of disease-stricken patients. Evidence has demonstrated that many of the mutations that make patients vulnerable to early onset amyloid disease function by increasing the probability of protein aggregation. Aging appears to be the most significant risk-factor, due to associated deficiencies in proteostasis and activation of stress-response signaling pathways. The similarity in aggregation of specific misfolded proteins that form insoluble fibrils leads researchers to investigate common pathways—like proteasome dysfunction and oxidative stress—in pursuit of targeted therapies for multiple amyloidosis types (Solomon et al. 2012).

It is believed that the process of amyloid fibril formation, known as amyloidogenesis, causes the decline of post-mitotic tissue characteristic of amyloid diseases (Johnson et al., 2005, Bucciantini et al., 2002, Hammarstrom et al., 2001, Hammarstrom et al., 2003, Lashuel et al., 2002, Walsh et al., 2002, Walsh and Selkoe, 2007). Amyloid fibrils form late in amyloid diseases and can disrupt cell and tissue structure in the extracellular space. However, the proteotoxicity of oligomers—which are formed earlier during amyloidogenesis—have cytotoxic effects and therefore may be the primary cause of these diseases (Solomon et al., 2012). It has been of great interest to

understand how amyloid fibrils form and how this leads to amyloid diseases like AD and PD.

There are a few hypotheses explaining the toxicity of amyloid fibrils, one being that the hydrophobic surfaces exposed in pre-amyloid intermediates aggregate structures that contain important cellular proteins and possibly compromising a multitude of cellular signaling pathways and physiological processes (Olzscha et al., 2011). This loss of function can explain the lack of integrity in the post mitotic tissue, which are made up of cells after cell division that have permanently stopped dividing, and do not easily regenerate. In addition, other hypotheses state that the amyloid and its precursors gain a new aberrant cellular function by unregulated ion channels or interfering with cellular traffic (Solomon et al., 2012).

### **History of Hereditary GSN Amyloidosis**

Hereditary Gelsolin Amyloidosis (HGA) has been characterized as an autosomal dominant inherited form of systemic amyloidosis (**Figure 3**). Clinical characteristics were first described by Finish ophthalmologist Jouko Meretoja in 1969 and was referred to as “Meretoja’s syndrome” (Meretoja, 1969). It was first reported that ten patients from three families studied displayed similar symptoms that were dominantly inherited, including lattice dystrophy of the cornea as well as cranial and peripheral neuropathy (Meretoja, 1969). It was not until 1990, that the novel amyloid fibril protein found in patients was identified as degradation fragment of gelsolin, an actin-binding protein,

resulting from a single base mutation found at nucleotide G654A from the gelsolin gene (*GSN*) (Levy et al. 1990; Maury et al. 1990). This single nucleotide substitution in the *GSN* gene was found to substitute aspartate at residue 187 to asparagine (D187N) (Levy et al. 1990; Maury et al. 1990). Additionally, in 1992, it was discovered in two families—Danish and Czech—a distinct G654T mutation, predicting a D187Y substitution. Different haplotypes (genetic backgrounds) in the two families suggest independent origins of the D187Y mutation, unlike the shared Finnish founder effect for D187N (de la Chappelle et al. 1992).

It has been thought that because these population groups are stable and have experienced only a small amount of immigration, their genome is augmented with several rare disease-causing genes (Solomon et al., 2012). It is estimated that there are 1000 carriers of HGA in Finland. Today, HGA is found in a number of countries including the United States, Japan, Portugal, England, Germany, Spain, France, Brazil, Sweden, Denmark, and the Czech Republic (Solomon et al., 2012)

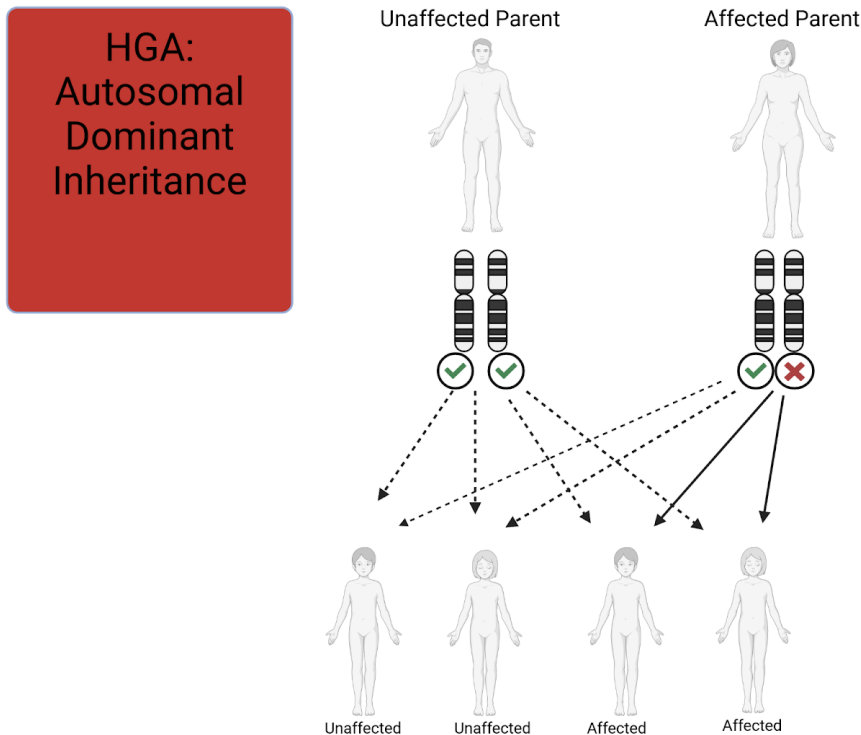


**Figure 3. Representation of Autosomal Dominance in HGA.** Due to its dominant nature, it can be passed from one generation to the next with 100% penetrance.

### Gelsolin Function

Gelsolin (GSN) is an abundant, calcium-activated, actin-modulating protein that is involved in many biological processes including filament assembly, stabilization, and disassembly (Kramer, 2016; Kiuru-Enari & Haltia, 2013). GSN comprises six domains (G1-G6) with binding sites for calcium (G1-G6), actin (G1, G4-G6), and PIP2 (G1-G3), and cleavage sites for furin (G2) and caspase-3 (G3-G4 linker) (**Figure 4**). Intracellularly, PIP2 binds G1-G3 to inhibit actin severing, regulating the dynamics of the cytoskeleton

until  $\text{Ca}^{2+}$  or PIP2 hydrolysis activates GSN (Janmey et al. 1987). Caspase-3 cleaves at D352 during apoptosis, yielding a pro-apoptotic G1-G3 fragment (~41 kDa) and accelerates actin breakdown (Kothakota et al. 1997).

When attached to the (+) end of an actin filament, GSN caps the protein and prevents depolymerization; however, when bound to the (-) end it promotes nucleation, but when bound in between these two extremities, it acts as a severing protein (Kramer, 2016) (**Figure 5**). In addition, GSN also functions in cell motility, signaling, apoptosis, as well as anti-scavenging and anti-inflammatory effects in the extracellular space (Bucki et al., 2008). Evidence has even shown its potential as an inhibitor of  $\text{A}\beta$ -generation in AD (Antequera et al., 2009). GSN's functions are primarily characterized within cells as an actin-binding regulator, but its alternatively spliced isoform, secreted as plasma gelsolin, is the established source of amyloid fibrils in hereditary gelsolin amyloidosis HGA (Chen et al. 2001).

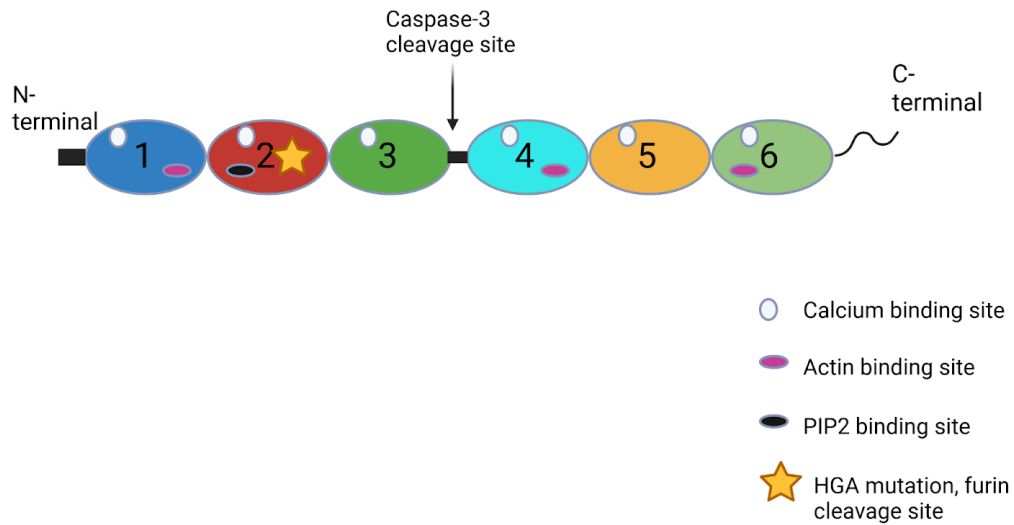


**Figure 4. Structure of Gelsolin.** Gelsolin (GSN) comprises six homologous domains (G1–G6), each contributing to its functionality through binding sites for calcium (multiple sites across G1–G6), actin (primarily G1, G4–G6), and phosphatidylinositol 4,5-bisphosphate (PIP2, G1–G3). Additionally, GSN contains two key cleavage sites: a furin cleavage site in G2, associated with the D187N mutation in hereditary gelsolin amyloidosis (HGA), and a caspase-3 cleavage site located in the linker between G3 and G4.

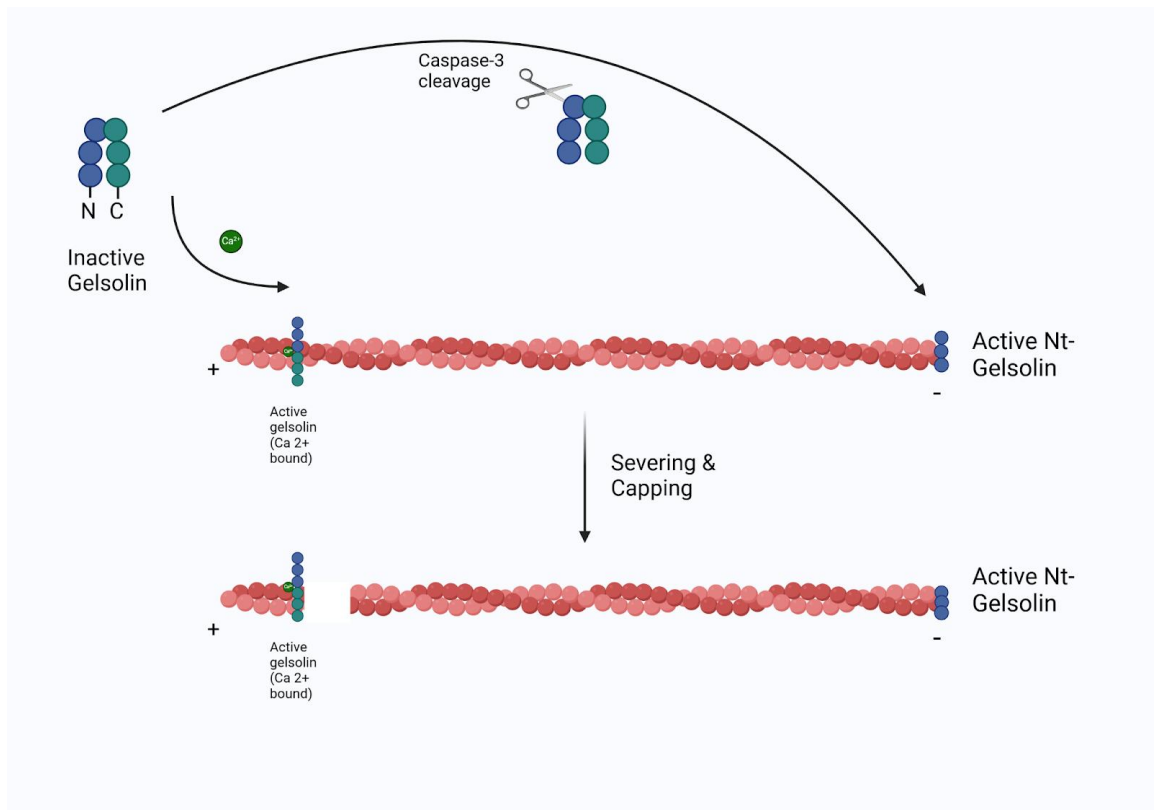


**Figure 5. Model of Gelsolin contribution to actin filament severing.**

## Genetics

The *GSN* gene, located on chromosome 9q33.2, spans approximately 70 kb in length and consists of 14 exons (Kwiatkowski et al., 1988; Maury et al., 1990). Alternate splicing of the *GSN* gene at exon 4 generates 2 isoforms— a cytoplasmic form (731 a.a.) that skips exon 4 and a secreted form (751 a.a.) that includes exon 4's signal peptide— both of which are affected by the D187N mutation (Kwiatkowski et al., 1988). A missense point mutation in the *GSN* gene at G654A or G654T at chromosome 9q32-34 is

the cause of this autosomal dominant inherited disease (Oregel et al. 2018). Point mutations typically destabilize normally folded proteins, thus leading to a higher concentration of partially denatured proteins that will become more efficient at aggregating (Solomon et al., 2012).

In HGA patients, amyloid fibrils accumulate in tissues and consist of abnormal gelsolin fragments, resulting from internal degradation of the protein carrying the D187N mutation (Haltia et al. 1990; Maury and Baumann, 1990). This mutation has been seen in all HGA patients in Finland, where the disease was first discovered (Kiuru, 1998). Wild-type plasma GSN is not associated with any amyloid pathology. However, D187N or D187Y mutation will grant 100% penetrance of HGA; therefore, making it a gain-of-toxic-function disease (Chen et al., 2001; Solomon et al., 2012).

### **Biochemistry**

Human GSN is expressed as both intracellular (81 kDa) and a secreted protein, known as plasma GSN (83 kDa) (Chen et al., 2001). HGA patients also display additional 60-70 kDa fragments, as opposed to the normal full-length 83 kDa fragments seen in healthy control individuals (Kiuri-Enari & Haltia, 2013). Plasma GSN is a precursor protein of HGA consisting of six domains (G1-G6) (**Figure 6**). The replacement of Asp at position 187 for Asn in domain G2 will result in abnormal intermediate protein conformation due to compromised calcium ( $\text{Ca}^{2+}$ ) binding (**Figure 7**). This cause the calcium binding site to be compromised and will lead to unusual proteolysis of the

uncovered cleavage site for  $\alpha$ -GSNase, furin, and ultimately lead to protein misfolding and amyloid fibrils formation (Solomon et al., 2012). Both forms of intracellular and extracellular GSN can lead to formation of major (173-243) and minor (173-225) amyloidogenic fragments from domain 2; however, literature suggests that the extracellular (secreted) plasma form is the most common (Chen et al., 2001).

It has been analyzed that the D187N/Y HGA-associated variants of plasma GSN reveal an initial proteolytic cleavage at position R172-A173 via  $\alpha$ -GSNase- which occurs in the Golgi. This will lead to production of a 68 kDa secreted C-terminal fragment (amino acids 173-755) of plasma GSN which will form oligomers. A second cleavage will occur at position M243-L244 of the C68 fragment via  $\beta$ -GSNase, producing 8 and 5 kDa amyloidogenic fragments that occur outside of the cell, forming fibrils and depositing systemically (**Figure 8**) (Solomon et al. 2012).

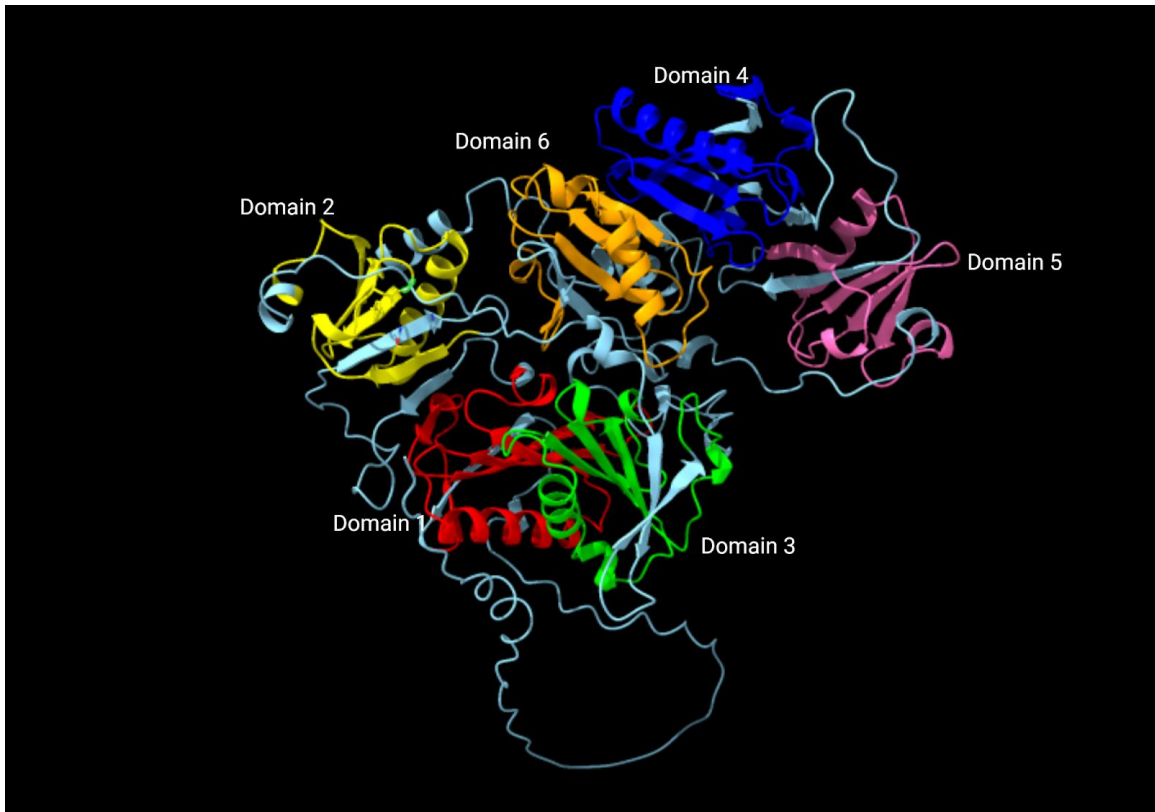


**Figure 6. Protein structure of Human GSN.** Protein consisting of six homologous domains (G1-G6). Gelsolin contains six calcium binding sites: G1& G2 (type 1; high affinity) and G3-G6 (type 2; low affinity) (Chen et al. 2001; Burtnick et al. 2004; Nag et al. 2009; PDB: 3FFN).

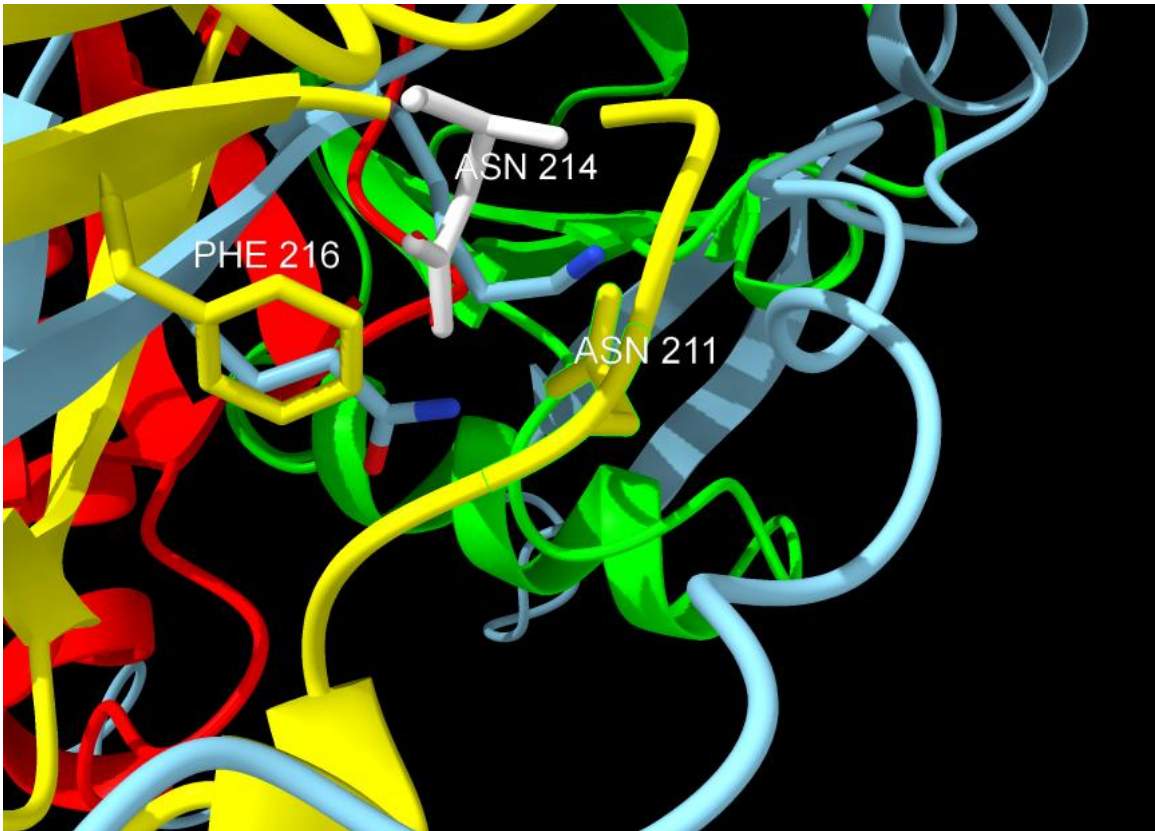


**Figure 7. Close-up of mutation D187N.** Also referred to as D214N when signal peptide is included, domain 2 of human GSN is a region critical for calcium binding and proper protein folding. The D187N mutation destabilizes the GSN protein, reducing  $\text{Ca}^{2+}$  binding, disrupting hydrogen bonding and causing steric clashes with neighboring residues, which promotes misfolding and amyloidogenic cleavage (Chen et al. 2001).

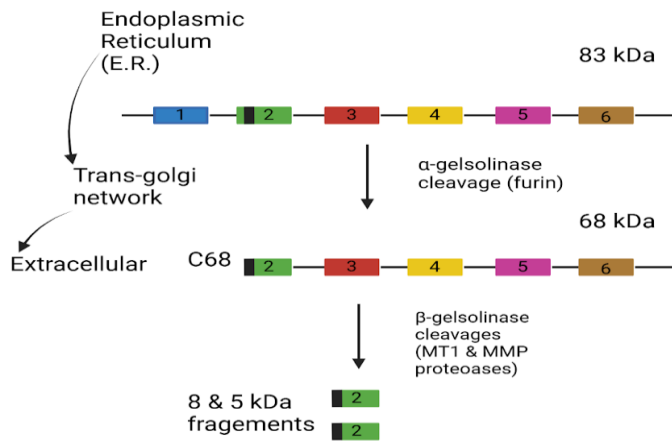


**Figure 8. Schematic representation of aberrant proteolyzation of plasma GSN.** Two protein enzymes- $\alpha$ -GSNase (Furin) and  $\beta$ -GSNase (MT1-MMP like proteases)- yielding 68 kDa and 5 & 8kDa, respectively.

### Clinical observations

HGA is also known as lattice corneal dystrophy type II (LCD2) and familial amyloidotic polyneuropathy (FAP) type IV; however, HGA is unlike other forms of familial amyloidosis clinically, pathologically, and biochemically. In its clinical heterogeneous form, it has been distinguished by adult onset of slowly progressive neurological, ophthalmologic, and dermatological symptoms, which includes corneal lattice dystrophy, cranial neuropathy and cutis laxa (Latin: “loose skin”) (**Figure 9**) (Kiuru-Enari & Haltia, 2013; Mendelson, 2023). Meretoja (1973) found that the first

clinical presentation of HGA is often corneal lattice dystrophy because of GSN amyloid deposition in the eye in the third decade of life. Congo red is used to detect amyloid deposition in the cornea—specifically in the anterior and middle stroma—as well as conjunctiva, sclera, and nerves and vessels of the eye (Solomon et al., 2012). When bound to the amyloid fibrils, Congo red will give the characteristic of apple-green birefringence when viewed under polarized light (**Figure 10**) (Mendelson et al. 2023).

The disease will slowly progress from the eye and affect the cranial and peripheral nerves, developing into a polyneuropathy (Solomon et al., 2012). Meretoja (1973) observed that the upper branch of the facial nerve is initially affected in HGA, with progression leading to the involvement of the lower branches. This manifestation is universally found in the HGA population. In addition, the trigeminal, glossopharyngeal, and hypoglossal nerves are affected, resulting in reduced sensation, reflex, tongue atrophy, fasciculations, dysarthria (motor speech disorder), and drooling (Kiuru, 1998).

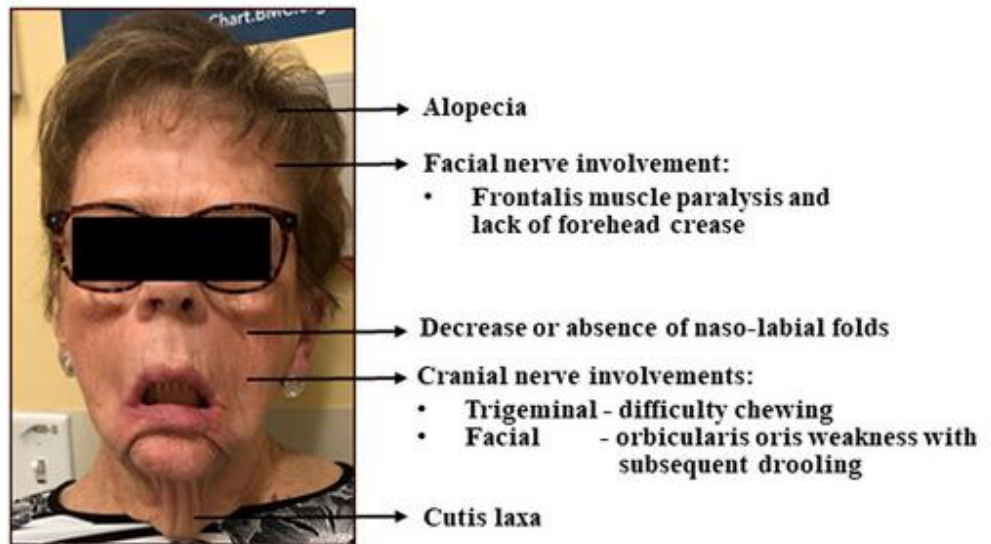


**Figure 9. Patient with various clinical manifestations relating to HGA** (Mendelson et al. 2023).

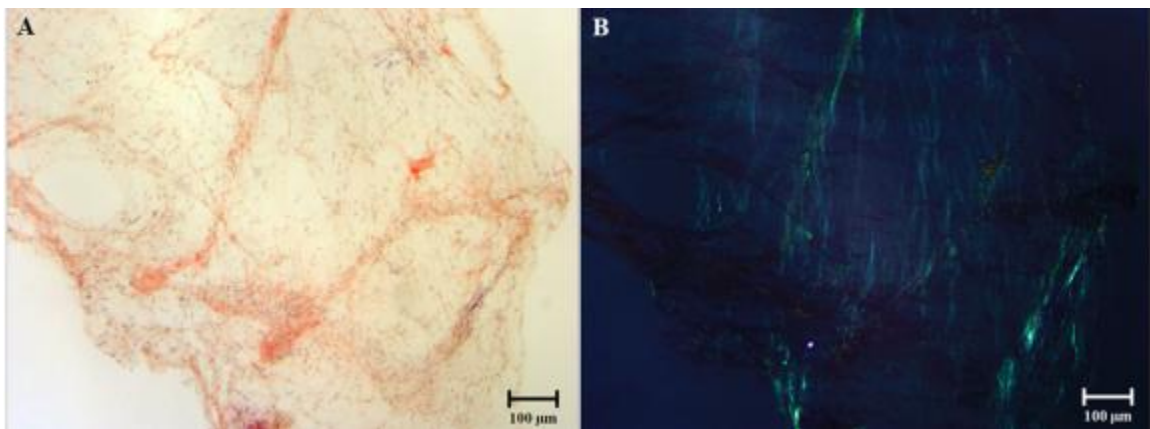


**Figure 10. Histological analysis of fat tissue of patient with HGA.** (A) Shows positive congo red stain of amyloid deposits. (B) Polarized light view showing green birefringence of congo red amyloid deposits (Mendelson et al. 2023).

Patients can also become ischemic due to deposition of amyloid into the vasculature as well as peripheral abnormalities (sensory) that affect the lower extremities (Kiuru-Enari et al., 2002). In terms of autonomic dysfunction, GSN fragments deposition in the autonomic nervous system can present as orthostatic hypotension (Kiuru et al., 1994; Makioka et al., 2010). Solomon et al. (2012) claim that it is likely that amyloid deposition in the vasculature could reduce arterial compliance and lead to dysregulated blood pressure.

Dermatologic abnormalities will be present with GSN amyloid also being found in the basement membrane of the skin, causing cutis laxa or loosened or thickened skin resulting in reduced elasticity and resilience (Kiuru- Enari et al., 2005). The sweat glands and hair follicles can be affected by GSN amyloid deposits, which will result in hair loss, itchy and dry skin, as well as intracutaneous bleeding (Kiuru et al., 1994; Makioka et al., 2010). Organs affected by GSN amyloid deposition in later stages and includes the kidney-with the homozygous mutation of GSN leading to severe nephrotic syndrome, causing proteinuria, and ultimately, end-stage renal failure (Maury, 1993). Lastly, GSN amyloid can be found in other vital organs and microvasculature, which can be life-threatening with causes including nephrotic syndrome, pneumonia (bulbar muscle dysfunction), and cerebral hemorrhage via cerebral angiopathy as the primary causes of death (Kiuru, 1998).

## Variants

There have been several amyloidogenic variants of GSN that have been identified, but the most common mutants are present in the G2 domain and are the only ones that are well characterized with a clear understanding of the mechanism (Bollati et al., 2021). The most common forms of HGA are caused by substitutions in G2, like D187N/Y mutations—resulting in systemic progressive deposition of amyloids. There are also other known mutations like N184K and G167R that are associated with deposits localized to the kidney (Bollati et al., 2021). Nonetheless, little is known behind the pathological mechanisms behind recently identified HGA forms. Most of the GSN mutations have been occurring on exon 4 and affecting the second domain.

Recently, a novel variant was discovered and featured unique genetic, biochemical and clinical features, that differed from the most common variant of HGA, D187N. A direct DNA sequencing found on exon 10 for *GSN* gene a heterozygous transition T to C transition at the first position of the TAC codon 447, c.1420T > C, coding for p.Y474H GSN variant protein. No mutation was found on exon 4 (Mendelson et al. 2023). Clinical features included mild bilateral carpal tunnel syndrome (CTS) and GSN amyloid deposits in the right breast tissue, a unique phenotype; however, no evidence of polyneuropathy, cranial, or ophthalmologic manifestations typical of HGA amyloidosis was observed. The Y447H replacement resides within the 4th domain and is not directly involved in calcium binding (Mendelson et al. 2023).

Interestingly, researchers at Boston University identified a patient with a second novel GSN variant, a mutation within exon 10, prompted by cranial neuropathy leading

to *GSN* gene testing. *GSN* amyloid deposits in glomerular tissue were also represented as a clinical manifestation, confirmed through microdissection of kidney samples. Using partial sequence chromatograms of exon 10, they detected a nucleotide substitution, c.1441C > T, resulting in a p.Arg481Cys (R481C) amino acid change (equivalent to R454C in cytoplasmic numbering) (Prokaeva, unpublished).

It is not known whether novel variants cause amyloidosis in the same way as the better characterized D187N, or if they experience alternative amyloidogenic pathways. In addition, more work needs to be done to evaluate these variants' folding stability, aggregation, and proteotoxic potential, as well as understanding the consequences of substitutions on the dynamics and structure of the protein (Bollati et al., 2021).

### **Goal of Research**

This study aimed to elucidate the molecular basis of gelsolin amyloidosis by analyzing full-length gelsolin and its isolated domain 4 (G4) from wild-type (WT) *GSN* and two G4 variants, Y447H and R454C. Drawing on the D187N variant in domain 2 (G2), which destabilizes gelsolin, undergoes furin cleavage into the amyloidogenic 68 kDa fragment (C68), and aggregates in hereditary gelsolin amyloidosis (HGA) (Chen et al., 2001), we hypothesized that Y447H and R454C similarly destabilize G4. As protein destabilization and aggregation are hallmarks of amyloidosis, we predicted these mutations would reduce expression, thermostability, and protease resistance relative to WT, potentially yielding C68 via a similar proteolytic pathway. WT *GSN*, evolved for optimal folding and stability, was expected to exhibit higher expression and greater

resistance to proteolysis than the variants, which we anticipated would degrade more rapidly due to structural instability or altered protease sites. To test this, we generated recombinant *GSN* constructs and assessed their expression and limited proteolysis via SDS-PAGE and Western blot with anti-gelsolin antibodies. Biophysical properties—including secondary structure and thermostability (far-UV CD spectroscopy), and the effect of EDTA and Ca<sup>2+</sup> binding on stability (CD and fluorescence spectroscopy)—were also evaluated to probe variant-specific differences.

## **METHODS**

### **Chemicals and Reagents**

Plasmids with human wild type (WT), Y447H (YH), R454C (RC) *GSN* encoding sequences were purchased from GenScript Biotech (Piscataway, NJ).

### **Site Directed Mutagenesis**

The pQE-1 plasmid with a DNA sequence optimized for expression in *E. coli* of N-terminal Methionine-Lysine-Histidine<sub>6</sub> (MKH<sub>6</sub>)-tagged human *GSN* domain 4 for WT, Y447H, and R454C used for site directed mutagenesis. The CMV5 plasmid with a DNA sequence optimized for expression in a Mammalian promoter system was used for WT, Y447H, R454C full-length *GSN* protein. A QuickChange II Site-Directed Mutagenesis Kit (Invitrogen/Thermo Fisher Scientific, Waltham, MA) was used to produce CMV5

and pQE-1 plasmids, for full-length and domain 4, respectively, each encoding for GSN variants WT, Y447H, and R454C.

#### **Bacterial Culture/Purification (Domain 4)**

2 L flasks with .5 L distilled water and 12.5 gs of LB media were made and placed in an autoclave. After, 500  $\mu$ L of ampicillin (Amp) was added to each autoclaved flask and placed in an incubator set at 37°C and shaking at 225 rpm overnight. Culture colonies were grown on LB agar petri dishes for proteins of the GSN. A colony was picked using a plastic scooper and put in 5 mL starter cultures and in addition to the flasks, were incubated overnight as well (37°C, 225 rpm). The following morning, two 5 mL of these starter cultures were inoculated (10 mL total) in each flask and continued to grow in the incubator for 2 hrs. The flasks optimal density was measured at an absorbance of 600 nm ( $OD_{600}$ ) until it reached between 0.4 to 0.6. Once this point was reached, we added 500  $\mu$ L of 0.5M of Isopropyl  $\beta$ -D-1-thiogalactopyranoside (IPTG) to induce protein expression for 3 hrs. After, the media was transferred to centrifuge bottles—each flask equally split into two bottles—and spun down at 10,000gs for 30 mins at 4°C. After being centrifuged, media was discarded, replaced with PBS, then placed in the freezer at -20°C. The next day proteins were spun down, supernatant was discarded, and sonication steps began.

Proteins were purified by binding of the N-terminal 6-His tagged proteins to Ni-bound agarose. Cell pellets were thawed on ice for 15 minutes and resuspended in an immobilized metal ion affinity column (IMAC) cell lysis buffer containing 1 mg/mL of lysozyme. The buffer/pellet ratio was 3mL/g wet weight, these suspensions were left on

ice for 30 minutes. Cells were sonicated while on ice over a 2 min interval, 15 sec increments for each pellet to control overheating, then centrifuged at 9,000 rpm and 4°C for 30 minutes. Supernatant was filtered through a 0.22 µm syringe tip filter into a 50 mL conical tube.

An IMAC column with 2 mL of Ni-NTA agarose was equilibrated using 40 mL of PBS (10x diluted). Up to 20 mL of cell lysate was loaded onto the column and rocked at room temperature for 1 hr. Flow-through was discarded and the column was washed with an IMAC buffer until the OD 280 nm was zero. The IMAC elution buffer was passed through the column and collected in 1 mL measures. Those that had OD 280 nm > 0.5 were collected. To exchange buffers, an Econo-Pac 10DG desalting column (Bio-Rad, Hercules, CA) was used and equilibrated in sample buffer, and loaded with 3 mL of IMAC-eluted sample having an approximate protein concentration of 2 mg/mL. Protein was exchanged into 4 mL of sample buffer. Concentration of proteins was calculated from measurement of UV absorption at 280 nm using the extinction coefficient of 19,940 M<sup>-1</sup>cm<sup>-1</sup> (Y447H) and 21,430 M<sup>-1</sup>cm<sup>-1</sup> (WT and R454C). Protein samples were aliquoted, flash frozen, and stored at -80 °C.

### **QIAprep® Spin Miniprep/DNA extraction (full length plasmids)**

Procedure began with 5 mL bacterial culture incubated overnight at 37°C and shaking 225 rpm. The following morning, these bacterial cultures were spun down and pelleted at 5000 rpm for 5 mins at room temperature (15-25°C). These pellet cells were

resuspended in 250  $\mu$ L Buffer P1(resuspension) and transferred to a microfuge tube. Following, P1, 250  $\mu$ L of Buffer P2 (lysis) was added and mixed until solution became clear. Then, 350  $\mu$ L Buffer N3 (neutralization) was added and mixed in similar fashion. Once mixed, we centrifuged for 10 minutes at 13,000 rpm. After, 800  $\mu$ L was collected and applied to QIAprep 2.0 spin column via pipetting. Once applied, the columns were spun down at 5000 rpm for 1 min. Buffers PB and PE, at 0.5 mL and 0.75 mL, respectively, were added as wash buffers and spun down at 5000 for 1 min. Finally, once columns were washed, they were transferred to sterile 1.5 mL microcentrifuge tubes, where 50  $\mu$ L Buffer EB was added to elute DNA. To measure concentration, a NanoDrop Lite Spectrophotometer from Thermo Fisher was used (Waltham, MA).

### **Mammalian Cell Culture/HEK293A**

**Table 1. Media**

<b>Reagent</b>	<b>Volume</b>
Dulbelcco's Modification of Eagle's Medium (DMEM)	225 mL
Fetal Bovine Serum (FBS)	25 mL
L-Glutamine 200 mM	5 mL
Penicillin/Streptomycin	1.25 mL

A Corning® Cell Culture Flask 75cm<sup>2</sup> (Corning, NY) was used for mammalian cell culture. Media was pre-warmed at 37°C in the incubator for 30 mins prior to putting 15 mL in the flask. A vial containing 1 mL of HEK293A adherent cells (1x10<sup>7</sup> cells/mL) retrieved from an -80-degree freezer, thawed on ice, then pipetted into the flask. Cells would grow until the flask reached 80-90% confluency, then passages would be made. We would transfect cells after they were allowed 2-3 passages to mature.

### **Transfection**

Once desired passages were made, cells were seeded on well plates (6-well: 0.22 x 10<sup>6</sup> cells; 24-well: 0.4x10<sup>5</sup> cells). Once cells were seeded, they were left in the incubator overnight at 37°C, 5% CO<sub>2</sub>. The next morning, the media was replaced with fresh media and placed in the incubator again for 1 hour. A GenJet™ In Vitro DNA Transfection Reagent (Gaithersburg, MD) was used to form Genjet-DNA complexes for transfection, where 1 µg of DNA was added in 50 µL DMEM (DNA solution) in microcentrifuge tubes, pipetted up and down, vortexed, then spun down briefly. Next, we added 3 µl of Genjet reagent to 50 µL DMEM (Genjet solution) in a separate microcentrifuge tube, pipetted up and down, vortexed, and spun down. Then we added 50 µl of Genjet solution to DNA solutions (Genjet/DNA complex), vortexed, spun down and incubated at room temperature for 15 minutes. Finally, Genjet/DNA complexes were added dropwise to plates, then placed back into incubators until it was time to retrieve

supernatants. Supernatants were concentrated using Amicon ® Ultra Centrifugal Filter, 10 kDa MWCO, until supernatant was concentrated to 2kDa.

### **Sodium Dodecyl Sulfate Polyacrylamide Gel Electrophoresis (SDS-PAGE)**

Supernatant was put into PCR tubes and denatured at 98°C for 7 minutes. Then supernatant was mixed with 2x SDS Tris-Glycine sample buffer and loaded on 8-16% Tris-Glycine 1mm gels (Waltham, MA). Precision Plus Protein Dual Color Standard ladder (Hercules, CA) was used along protein samples to measure size of proteins as they traveled through the gel. The gels were run under 140 volts for 1-2 hours at room temperature, then transferred onto a nitrocellulose membrane with a pore size of 0.2 µm (Bio-Rad) at 30mV and left overnight at 4°C cold room.

### **Antibodies and Developing Western Blots**

The next morning, membranes were removed from the transfer apparatus and placed in blot boxes with TBST. Next, the membranes were blocked with 5% milk (in TBST) for 1 hour. Membranes were washed with TBST 3x for 5 minutes each. Then, we diluted GSN primary antibodies (Waltham, MA) at 1:2000 in 2.5% milk, added to boxes, then incubated for 2 hours. After, membranes were washed again 3x for 5 minutes each. Then a secondary antibody (goat anti-rabbit HRP) was diluted at 1:4000 in 2.5% milk, added to boxes, then incubated for 1 hour. Finally, boxes were washed 3x for 5 minutes each. Blots were developed using a ECL Plus Western Blotting Detection System before

being imaged on an ImageQuant LAS 4000 and analyzed on the ImageQuant 4000 software.

### **Limited Proteolysis**

Limited proteolysis was performed using proteinase K (PK; 1 $\mu$ M). Two 15  $\mu$ L aliquots of sample were added put into two PCR tubes for each protein sample (WT, Y447H, and R454C), these were designated as time "0" A and B, then 1 $\mu$ L PMSF (1mM) and 1.5 PBS was added to compensate for the protease we added to the experimental samples (5, 10, 20, 30, 45, 60 mins). A working dilution of 1  $\mu$ M PK was made, samples were put in glass vials and pre-warmed to 37 $^{\circ}$ C in incubator, then 1  $\mu$ L of PMSF was added to each experimental PCR tube (2 repeats, 3 samples, 6 time points= 36 PCR tubes) that were chilled on ice (prevent evaporation). Then 16  $\mu$ L of PK was added to each sample in 20 second intervals, beginning the experiment, then 16.5  $\mu$ L of sample was taken at each time point and put into PCR tubes on ice. Once aliquots were collected, samples were mixed with 2x SDS loading buffer, denatured at 98  $^{\circ}$ C for 7 minutes, then loaded onto 8-16% Tris-Gly gel, transferred onto cellulose membranes overnight, immunoblotted with antibodies the following morning, where they were developed using a ECL Plus Western Blotting Detection System before being imaged on an ImageQuant LAS 4000 and analyzed on the ImageQuant 4000 software.

## RESULTS

### Expression of WT and Variant Gelsolin Constructs in HEK293A Cells

To investigate the molecular basis of gelsolin amyloidosis variants, recombinant constructs of WT and mutant GSN were generated to assess protein expression and detect the 68kDa fragments, an amyloidogenic proteolysis product implicated in HGA. In HGA, C68 arises from furin-mediated cleavage of misfolded gelsolin mutants, such as D187N, contributing to amyloid fibril formation (Chen et al., 2001). After constructs were made, HEK293A cells were adhered on a 24-well plate and transfected with plasmids using a GenJet™ lipo-based transfection reagent. Supernatant was collected 4 hours post-transfection. Full length GSN (~83 kDa) was stable across WT and variants during purification. However, we did not observe 68 kDa fragment bands, suggesting that there was no endogenous cleavage after 4 hours post-transfection. Despite no fragment detection, expression of all constructs enabled subsequent analysis of the C68 fragment formation across additional time points.

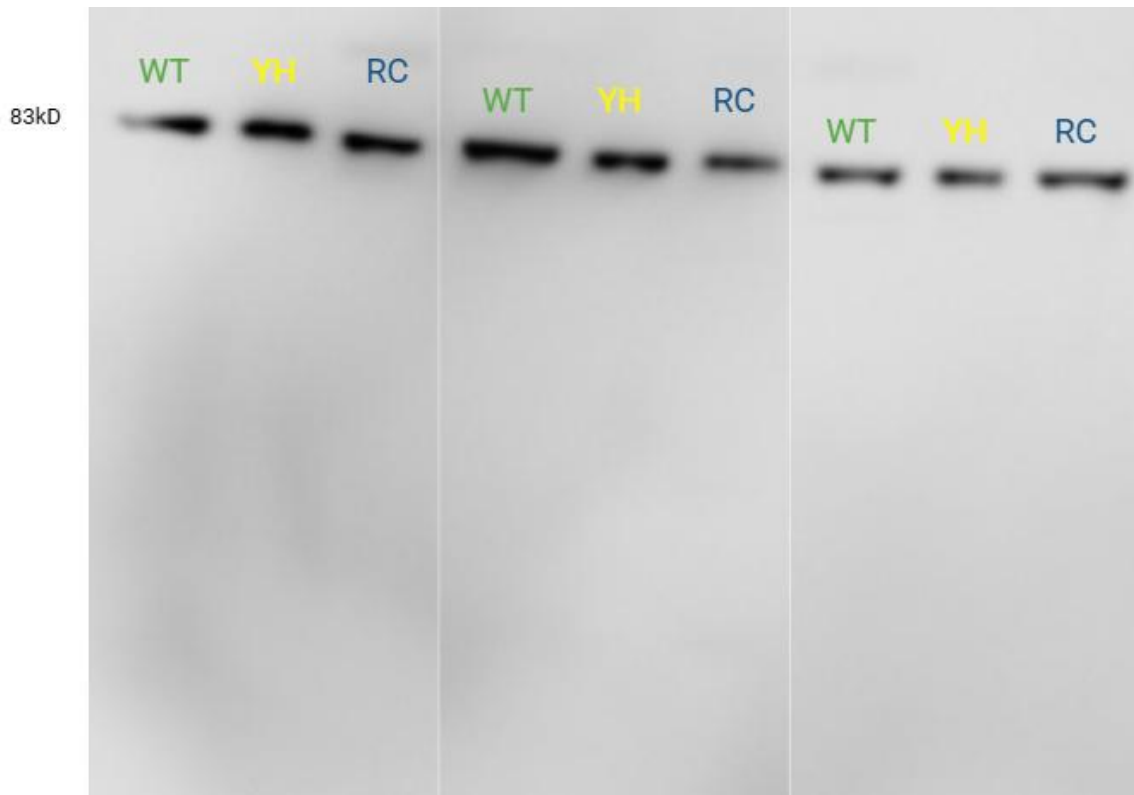


**Figure 11A. Western blot analysis confirming the successful expression for constructed Wild type (WT) GSN and variants- Y447H (YH) and R454C (RC).** WT and variant proteins were expressed in HEK293A cells transfected with 1  $\mu$ g plasmid. Supernatant, which was collected 4 h post-transfection from a 24-well plate, underwent SDS-PAGE on the same gel and was transferred to a cellulose membrane, then immunoblotted with an anti-GSN antibody. The expected bands corresponding to the WT and variants (~83kD) were detected.

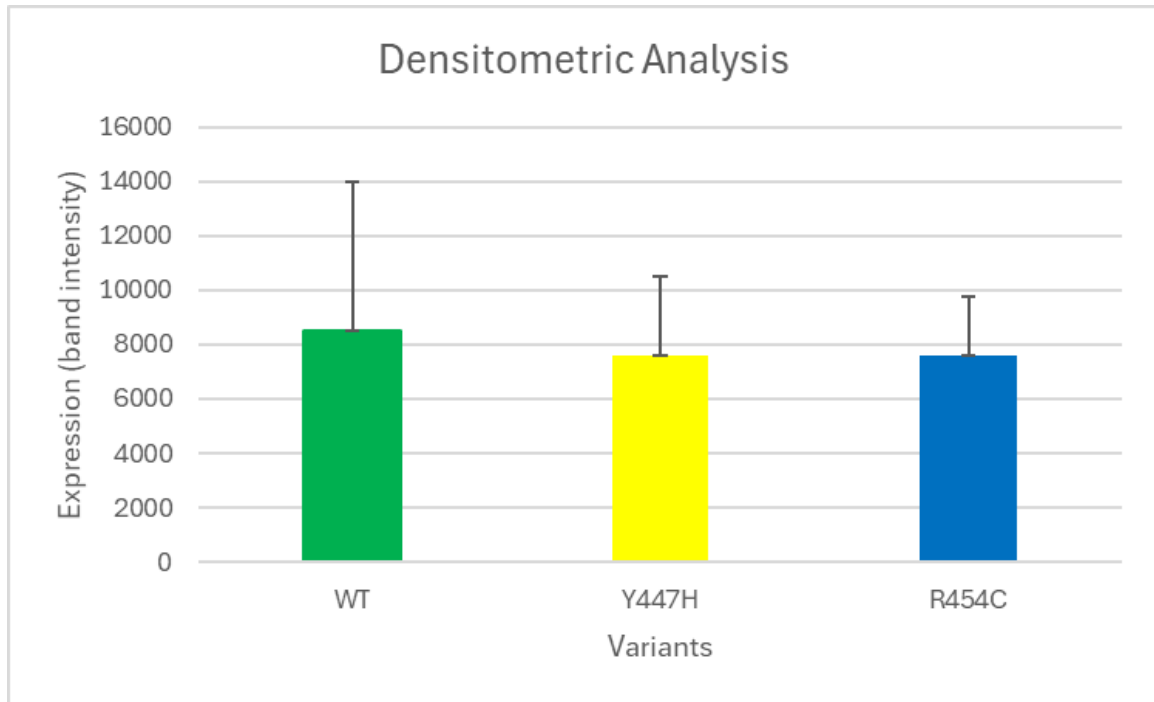


**Figure 11B. Densitometric analysis of WT and variant GSN protein expression in supernatant collected 4 hours post-transfection from a 24-well plate.** Western blot bands were quantified to assess extracellular protein expression for WT, Y447H, and R454C variants. Densitometry showed that both variants, Y447H and R454C, exhibited reduced extracellular expression compared to WT, which displayed the highest variability (SD = 5481.2 AU), though these differences were not statistically significant (ANOVA,  $p = 0.95$ ). Y447H exhibited the lowest expression, with greater variability than R454C (SD = 2936.6 vs. 2165.3 AU). \*AU= Arbitrary units for band intensity. Error bars represent the standard deviation.

### **Detecting 68 kDa Fragments in HEK293A Cells at Varying Time Points**

The next objective was to confirm whether these variants produce the 68 kDa C-terminal fragments across varying time points (4, 8, and 24hrs), which is a hallmark of gelsolin amyloidosis. The 68 kDa C68 fragment was analyzed in WT and variant GSN constructs, YH and RC, to determine if emerging mutations involved in the 4th domain exhibit processing like established amyloidosis variants in the 2nd domain.

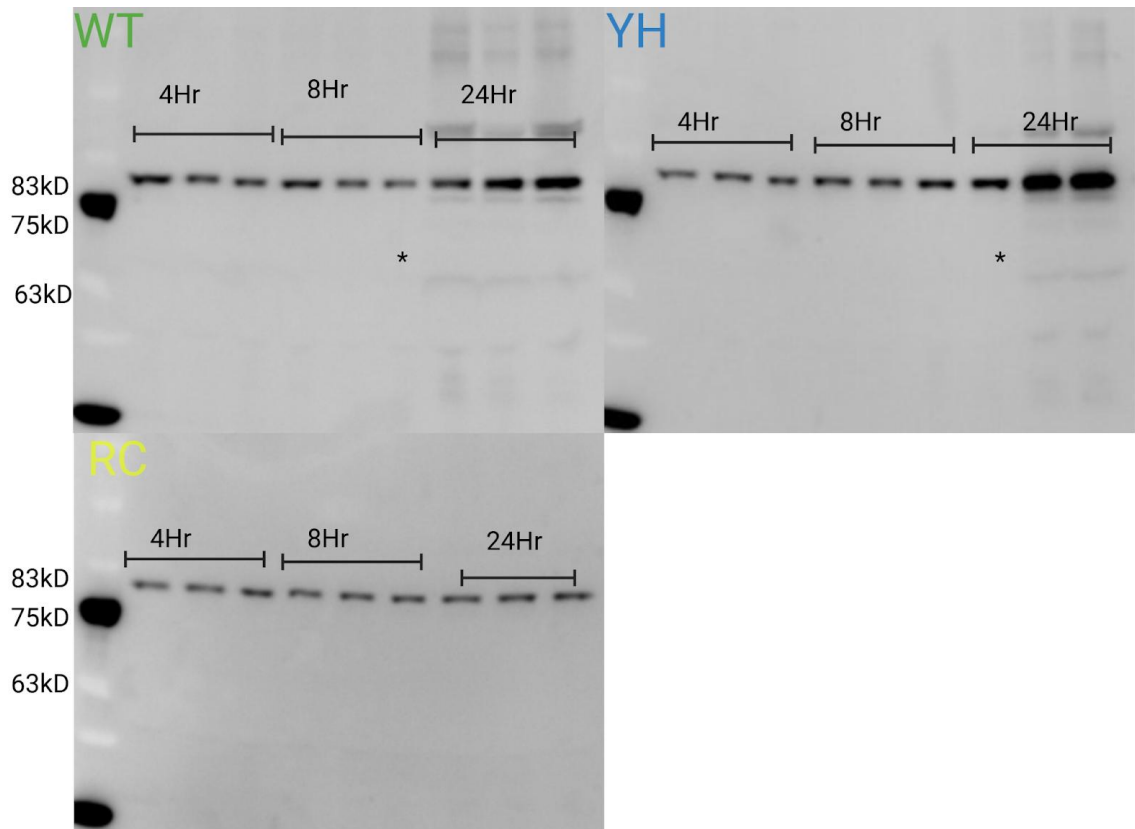


**Figure 12A. Time-course analysis of 68 kDa fragment expression in WT and variant GSN proteins at 4-, 8-, and 24-hours post-transfection.** WT and variant proteins were expressed in HEK293A cells transfected with 1  $\mu$ g plasmid, and supernatants were collected across each time course. Three supernatant repeats were collected from a 24-well plate, subjected to SDS-PAGE, and analyzed by Western blot using anti-GSN antibody. \*A band at ~68kDa was detected for YH; however, a similar banding pattern was detected at this position in the WT sample, suggesting that this band may be a non-specific signal or common processing product, rather than aberrant proteolytic activity.

Further analysis is needed of the identity of this fragment and its significance to the variant.

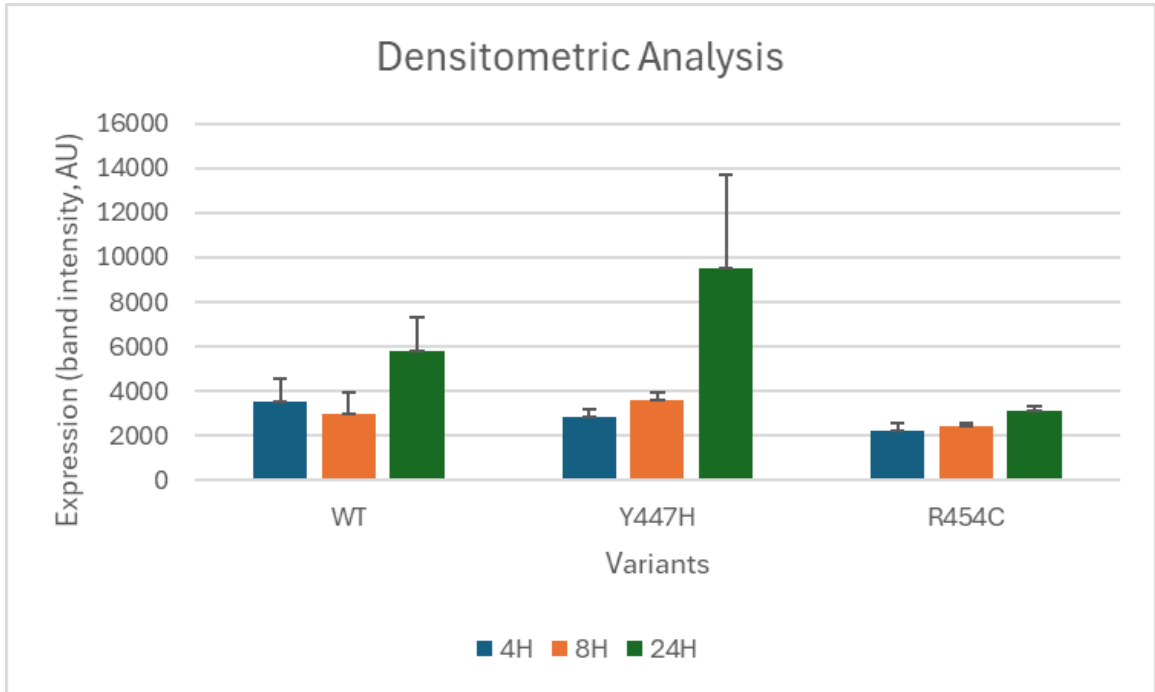


**Figure 12B. Densitometric analysis of full-length protein GSN expression in WT and variant proteins at 4-, 8-, and 24-hours post-transfection.** Western blots measure band intensity, expression levels for WT, Y447H, and R454C were quantified from separate gels, each containing all timepoints for a single variant ( $n = 3$  per time point). Band intensities are reported as mean  $\pm$  SD from densitometry, with comparisons limited to within each gel to avoid cross-gel exposure variability. WT showed a slight decrease from 4h to 8h, then an increase by 24h (ANOVA,  $p = 0.058$ ). Y447H exhibited a slight increase from 4h to 8h, then a significant increase by 24h ( $p = 0.028$ ). R454C displayed a gradual increase throughout the time course ( $p = 0.015$ ). Trends reflected temporal

changes within each variant, not absolute differences between variants. \*Error bars represent the standard deviation.

### **Limited Proteolysis Experiment and Stability Analysis**

The final experiment for the full-length GSN was to mimic disease-relevant processing by performing limited proteolysis. The goal of this experiment aimed to assess stability, cleavage patterns, as well as amyloidogenic fragment production in mutant GSN, Y447H and R454C.

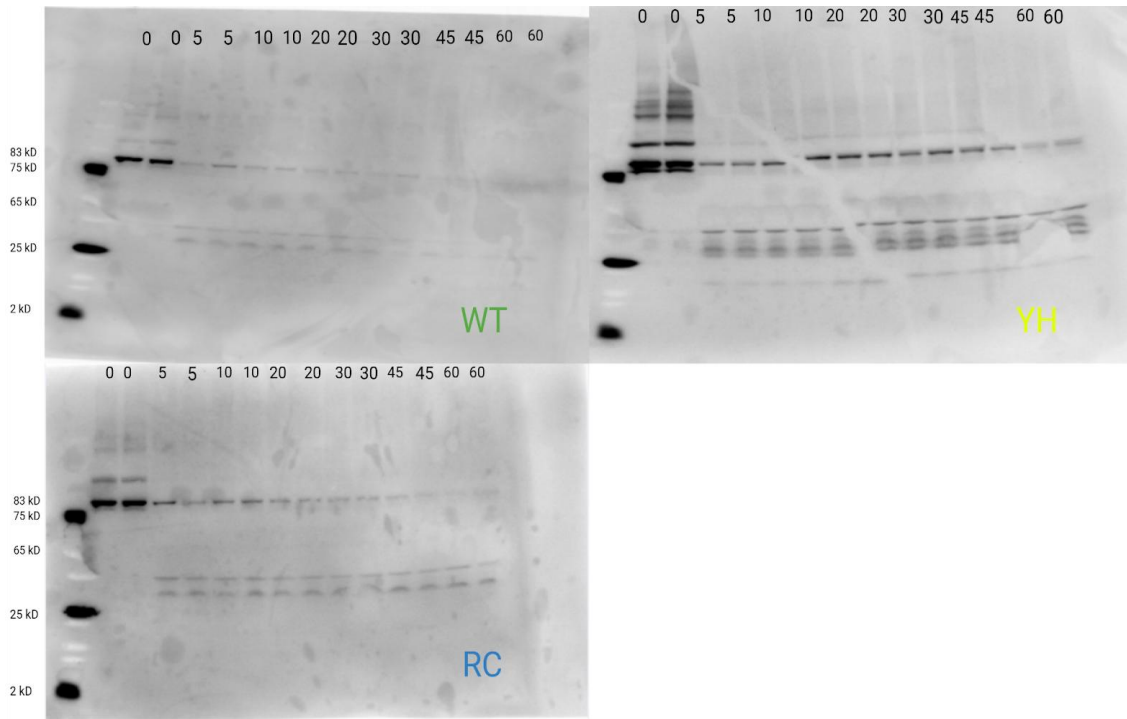


**Figure 13A. Proteolysis analysis of full-length WT and variant GSN proteins over seven time points.** WT and variant proteins were expressed in HEK293A cells transfected with 1  $\mu$ g plasmid, and supernatants were collected 24 hours post-transfection. Purified proteins were incubated with Proteinase K (1  $\mu$ M) at 37°C, with reactions quenched using PMSF (1 mM) at the end of each time point, time points “0” contained only PBS and protein. Samples were analyzed by SDS-PAGE and Western blot to assess the rate of full-length protein degradation.

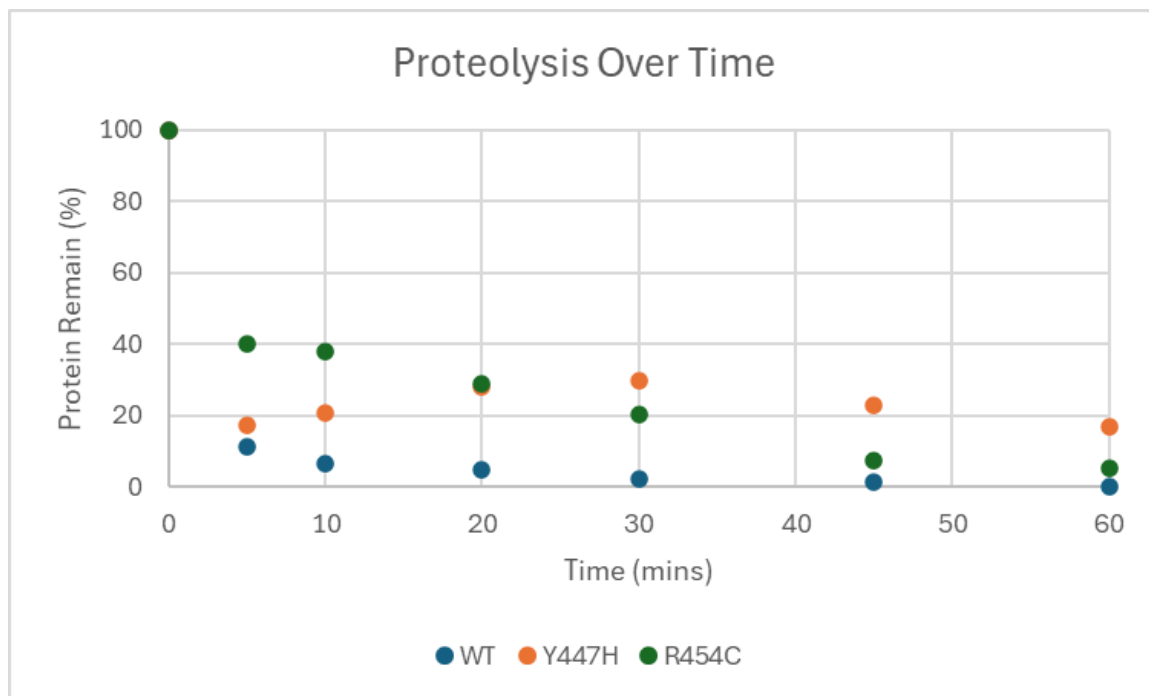


**Figure 13B. Time course analysis of limited proteolysis for WT and variant GSN proteins (Y447H and R454C).** Proteins were run on separate gels, protein percentage was calculated from Western blot band intensities normalized to each variant's zero baseline (0=100%) and plotted against time (0, 5, 10, 20, 30, 45, 60 min). Data represent averages of two replicates per time point. At 5 minutes, WT exhibited the fastest degradation (11.2% remaining), followed by Y447H (17.4%), and R454C (40.2%). By 30 minutes, Y447H exhibited the highest percentage remaining (29.7%), surpassing R454C (20.3%) and WT (4.3%, most degraded), despite its lower percentage at 5 minutes. At 60 minutes, WT appeared fully degraded (0%), followed by R454C (5.75%), then Y447H (16.95%, least degraded). This shift highlights Y447H's slower degradation rate over time compared to WT and R454C, though direct comparisons across variants are limited by potential exposure and loading variability between gels.

## DISCUSSION

In our initial experiment, recombinant constructs of wild-type (WT) GSN and variants Y447H and R454C were expressed in HEK293A cells (Figure 11A), where WT exhibited greater protein levels in supernatant at 4 hours post-transfection compared to the variants (Figure 11B). Although these differences were not statistically significant (ANOVA,  $p = 0.95$ ), the trend aligned with our hypothesis that WT, optimized for folding and stability, would outperform variant expression. In contrast, no 68 kDa (C68) fragments were detected in variant *GSN* (Y447H, R454C) at 4 hours post-transfection, nor at subsequent timepoints (8 and 24 hours; Figure 12A), contrary to our expectation of observing amyloidogenic proteolysis products like those in D187N-mediated gelsolin amyloidosis (Chen et al., 2001). This absence suggests limited cleavage under these conditions, potentially due to variant stability or insufficient time for C68 formation.

Interestingly, WT and R454C exhibited a gradual rise in protein levels, while Y447H showed a sharp increase by 24 hours (Figure 12B), conflicting to our expectation of reduced expression and amyloidogenic proteolysis akin to D187N-mediated gelsolin amyloidosis (Chen et al., 2001). This suggests that under these conditions, *GSN* variants resist cleavage into C68, potentially due to enhanced stability or insufficient protease activity. Our final experiment assessed the proteolytic stability of *GSN* variants (Y447H and R454C) compared to wild type (WT), alongside investigation of potential C68 fragment formation. After 60 minutes of limited proteolysis, WT was fully degraded, R454C showed intermediate degradation, and Y447H exhibited the greatest stability,

retaining significant protein levels (Figure 13 A&B). These findings indicate that Y447H and R454C are less susceptible to proteolysis than WT, with Y447H demonstrating superior resistance, possibly due to structural modifications in G4 that limit protease accessibility.

Dr. Elena Klimtchuk at the Amyloidosis Center, Boston University, contributed further biophysical and structural insights into domain 4 (G4) of GSN variants, supporting our stability and proteolysis findings. Circular dichroism (CD) spectroscopy analysis in the presence of EDTA, conducted by Dr. Klimtchuk, revealed that the secondary structure of GSN (G4) variants Y447H and R454C coincide that of WT, with negative ellipticity peaks at ~208 nm and ~222 nm, consistent with predominant  $\alpha$ -helical content (Figure 14; Klimtchuk, unpublished). These results suggest that G4 mutations retain helical folding even without  $\text{Ca}^{2+}$ , possibly explaining Y447H and R454C's resistance to proteolysis compared to WT after 60 mins (Figure 13A&B).

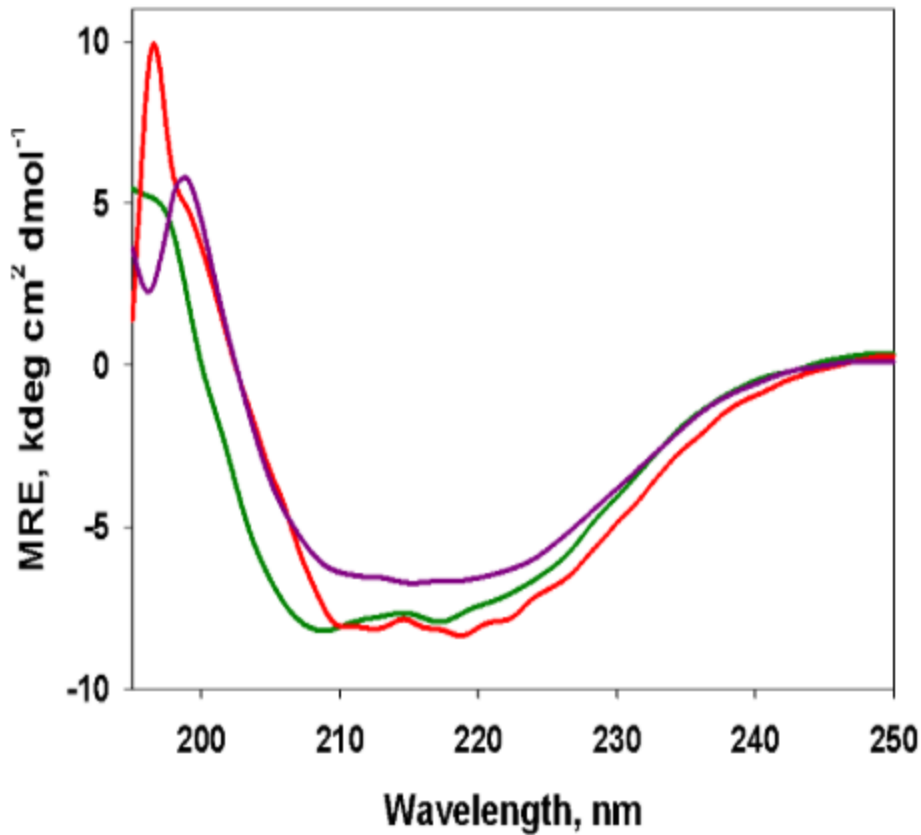


**Figure 14. CD spectra of recombinant GSN WT, Y447H and R454C proteins.** Far-UV CD spectra of WT (green), Y447H (red), and R454C (purple) at 25°C with N-terminal MKH<sub>6</sub> tags.

Thermostability analysis of GSN variants provided critical insights into G4 behavior under calcium-modulated conditions, expanding on our proteolysis findings. Using CD spectroscopy, WT exhibited a T<sub>m</sub> of 69°C with EDTA and 81°C with Ca<sup>2+</sup>, Y447H showed 67°C with EDTA and 85°C with Ca<sup>2+</sup>, and R454C displayed a T<sub>m</sub> of 84°C with EDTA but 78°C with Ca<sup>2+</sup> (Figure 14; Klimtchuk, unpublished). The significant calcium-induced stabilization in WT ( $\Delta T_m = +12^\circ\text{C}$ ) and Y447H ( $+18^\circ\text{C}$ )

indicates that calcium binding enhances G4's helical integrity, aligning with GSN's calcium-dependent folding (Kwiatkowski et al., 1988). Y447H's  $T_m$  of 85°C with  $Ca^{2+}$  aligns with its proteolytic resistance after 60 minutes (Figure 13 A&B).

### Thermostability of Gelsolin domain 4 with EDTA or $CaCl_2$

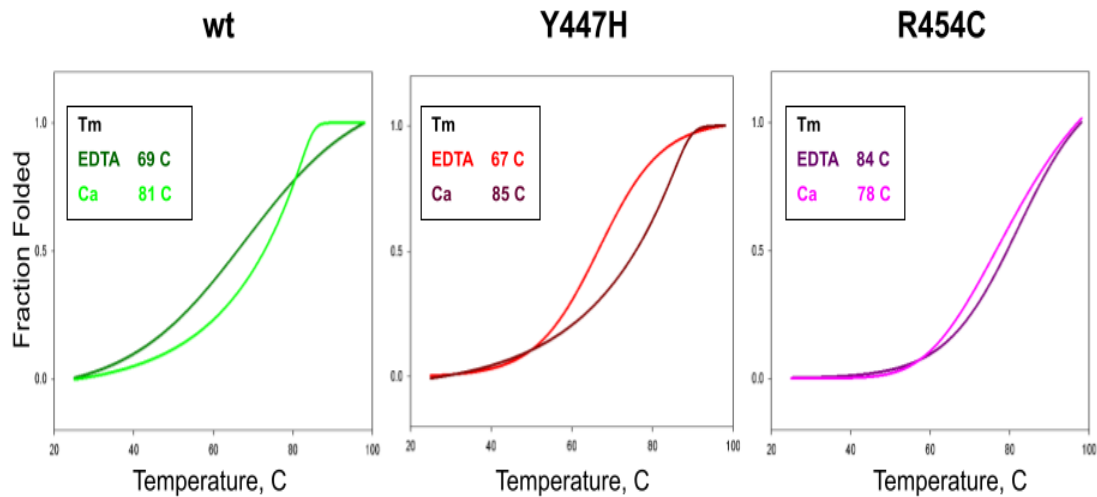


**Figure 15. Thermal stabilities of recombinant GSN wild-type and variant proteins, with N-terminal MKH 6 tags, assessed using CD spectroscopy.** Tagged wild-type, Y447H, and R454C analyzed by CD spectroscopy with monitoring at 218 nm during heating from 25 to 100 °C at a rate of 1°C/min. Melting curves for R454C did not plateau when experiment stopped at 100°C.

A final proteolysis experiment targeting G4 of GSN WT and variants Y447H and R454C, contrary to our earlier assay (Figure 13 A&B), revealed unique degradation profiles. It was found that WT had degraded the fastest, Y447H intermediate, and R454C with the slowest degradation and notable dimers on SDS-PAGE (Figure 16; Klimtchuk, unpublished).

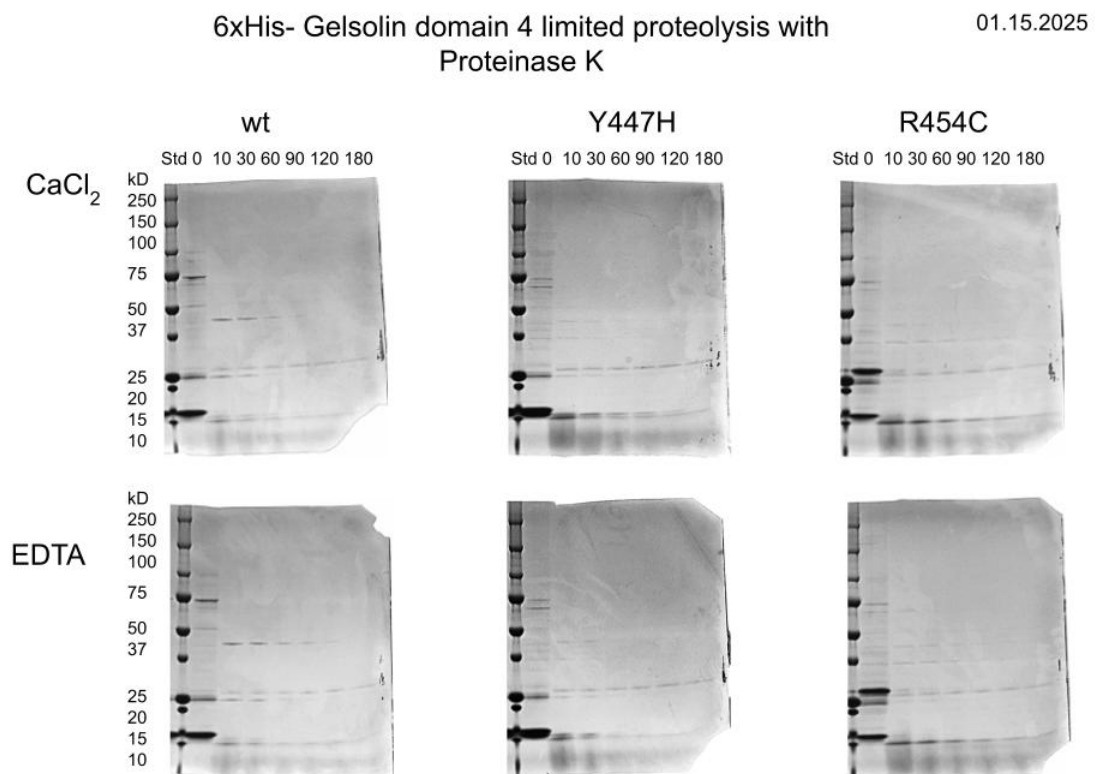


**Figure 16. Gelsolin Domain 4 Limited Proteolysis with Proteinase K.** WT and variants Y447H and R454C with N-terminal H<sub>6</sub> tags were treated with both EDTA and Calcium Chloride.

These findings contrast with our prior observation at 60 minutes, where WT was fully degraded, R454C intermediate, and Y447H most stable (Figure 13 A&B). The persistence of R454C dimers suggests that its cysteine mutation (R454C) forms stable disulfide bonds with neighboring residues, enhancing early resistance to proteases, consistent with its elevated  $T_m$  of 84°C in the presence of EDTA (Figure 15; Klimtchuk, unpublished data). This corroborates Dr. Klimtchuk's thermostability data, where R454C's stability exceeds WT (69°C) and Y447H (67°C) without  $Ca^{2+}$ , while Y447H's higher  $T_m$  with  $Ca^{2+}$  (85°C) aligns with its proteolytic resilience in prior conditions. In the context of HGA, R454C's dimerization may indicate a propensity for oligomeric states that resist initial cleavage into C68, unlike D187N's rapid G2 breakdown (Chen et al., 2001), though such fragments remain undetected here, underscoring the role of experimental conditions in shaping *GSN*'s fate.

In conclusion, contrary to our initial hypothesis, these data do not support the notion that G4 mutations Y447H and R454C destabilize domain 4 in a manner analogous to the D187N mutation's effect on domain 2 in hereditary gelsolin amyloidosis (HGA). Instead, Y447H's  $Ca^{2+}$ -dependent stabilization and R454C's dimer formation (Figure 15) indicate a distinct mechanism—potentially protective or redirective—highlighting that *GSN*'s association with amyloidosis depends on domain-specific mutational effects rather than global destabilization (Mendelson et al. 2023). Our findings indicate that G4 mutations may protect against HGA-like amyloidosis by stabilizing *GSN* or redirecting misfolding into non-amyloid oligomers, revealing variant-specific roles in disease modulation. These data align with models where destabilizing mutations (e.g., A $\beta$  and

prion) drive fibril formation, while stabilizing (Y447H) or redirecting (R454C) mutations mitigate pathology (Chiti & Dobson, 2017). Moreover, variant-specific  $\text{Ca}^{2+}$  effects on  $T_m$  (WT +12°C, Y447H +18°C, R454C -6°C) suggest that enhancing  $\text{Ca}^{2+}$  binding, as in Y447H, could offer a therapeutic strategy to prevent misfolding in HGA.

## REFERENCES

- Anfinsen CB. Principles that govern the folding of protein chains. *Science*. 1973 Jul 20;181(4096):223-30. doi: 10.1126/science.181.4096.223. PMID: 4124164.
- D. Antequera, T. Vargas, C. Ugalde, C. Spuch, J. A. Molina, I. Ferrer, F. Bermejo-Pareja, E. Carro, Cytoplasmic gelsolin increases mitochondrial activity and reduces A $\beta$  burden in a mouse model of Alzheimer's disease, *Neurobiology of Disease*, Volume 36, Issue 1, 2009, Pages 42-50, ISSN 0969-9961, <https://doi.org/10.1016/j.nbd.2009.06.018>. (<https://www.sciencedirect.com/science/article/pii/S0969996109001624>)
- Atkins, P. W., & de Paula, J. (2014). *Physical chemistry* (10th ed., pp. 92–97). Oxford University Press.
- Bollati M, Diomede L, Giorgino T, Natale C, Fagnani E, Boniardi I, Barbiroli A, Alemani R, Beeg M, Gobbi M, Fakin A, Mastrangelo E, Milani M, Presciuttini G, Gabellieri E, Cioni P, de Rosa M. A novel hotspot of gelsolin instability triggers an alternative mechanism of amyloid aggregation. *Computational and Structural Biotechnology Journal*. 2021 Nov 19;19:6355-6365. doi: 10.1016/j.csbj.2021.11.025. PMID: 34938411; PMCID: PMC8649582.
- Bucciantini M, Giannoni E, Chiti F, Baroni F, Formigli L, Zurdo J, Taddei N, Ramponi G, Dobson CM, Stefani M. Inherent toxicity of aggregates implies a common mechanism for protein misfolding diseases. *Nature*. 2002;416:507–511. doi: 10.1038/416507a.
- Bucki R, Levental I, Kulakowska A, Janmey PA. Plasma Gelsolin: Function, Prognostic Value, and Potential Therapeutic Use. *Current Protein & Peptide Science*. 2008; 9:541–551. [PubMed: 19075745]
- Burtnick, L. D., Urosev, D., Irobi, E., Narayan, K., & Robinson, R. C. (2004). Structure of the N-terminal half of gelsolin bound to actin: Roles in severing, apoptosis and FAF. *The EMBO Journal*, 23(14), 2713–2722.
- Bustamante JG, Zaidi SRH. Amyloidosis. [Updated 2023 Jul 31]. In: StatPearls [Internet]. Treasure Island (FL): StatPearls Publishing; 2025 Jan-. Available from: <https://www.ncbi.nlm.nih.gov/books/NBK470285/>
- Buxbaum JN, Eisenberg DS, Fändrich M, McPhail ED, Merlini G, Saraiva MJM, Sekijima Y, Westermark P. Amyloid nomenclature 2024: update, novel proteins, and recommendations by the International Society of Amyloidosis (ISA) Nomenclature Committee. *Amyloid*. 2024 Dec;31(4):249-256. doi: 10.1080/13506129.2024.2405948. Epub 2024 Sep 30. PMID: 39350582.

de la Chapelle, A., Tolvanen, R., Boysen, G., Santavy, M., Bleeker-Wagemakers, L., Maury, C. P. J., & Kere, J. (1992). Gelsolin-derived familial amyloidosis caused by asparagine or tyrosine substitution for aspartic acid at residue 187. *Nature Genetics*, 2(2), 157–160. <https://doi.org/10.1038/ng1092-157>

Chen CD, Huff ME, Matteson J, Page L, Phillips R, Kelly JW, Balch WE. Furin initiates gelsolin familial amyloidosis in the Golgi through a defect in Ca(2+) stabilization. *EMBO Journal*. 2001 Nov 15;20(22):6277-87. doi: 10.1093/emboj/20.22.6277. PMID: 11707399; PMCID: PMC125307.DOI: 10.1146/annurev.bi.60.070191.004051

Chiti, F., & Dobson, C. M. (2006). Protein misfolding, functional amyloid, and human disease. *Annual Review of Biochemistry*, 75, 333–366. <https://doi.org/10.1146/annurev.biochem.75.101304.123901>

Dill, K. A., & Bromberg, S. (2010). *Molecular driving forces: Statistical thermodynamics in biology, chemistry, physics, and nanoscience* (2nd ed.). Garland Science.

Dill, K. A., & Chan, H. S. (1997). From Levinthal to pathways to funnels: The "new view" of protein folding kinetics. *Nature Structural Biology*, 4(1), 10–19. <https://doi.org/10.1038/nsb0197-10>

Dobson, C. M. (2003). Protein folding and misfolding. *Nature*, 426(6968), 884–890. <https://doi.org/10.1038/nature02261>

Fändrich, M., Fletcher, M. A., & Dobson, C. M. (2001). Amyloid fibrils from muscle myoglobin. *Nature*, 410(6825), 165–166. <https://doi.org/10.1038/35065514>

GENCODE Consortium. (2025). GENCODE Release 45. *Ensembl Database*. Retrieved March 17, 2025, from [https://www.genecodegenes.org/human/release\\_45.html](https://www.genecodegenes.org/human/release_45.html)

Haltia M, Prelli F, Ghiso J, Kiuru S, Somer H, Palo J, Frangione B. Amyloid protein in familial amyloidosis (Finnish type) is homologous to gelsolin, an actin-binding protein. *Biochemical and Biophysical Research Communications*. 1990 Mar 30;167(3):927-32. doi: 10.1016/0006-291x(90)90612-q. PMID: 2157434.

Hammarstrom P, Schneider F, Kelly JW. Trans-suppression of misfolding in an amyloid disease. *Science*. 2001;293:2459–2462. doi: 10.1126/science.1062245.

Hammarstrom P, Wiseman RL, Powers ET, Kelly JW. Prevention of transthyretin amyloid disease by changing protein misfolding energetics. *Science*. 2003;299:713–716. doi: 10.1126/science.1079589.

Hartl, F. U., Bracher, A., & Hayer-Hartl, M. (2011). Molecular chaperones in protein folding and proteostasis. *Nature*, 475(7356), 324–332. <https://doi.org/10.1038/nature10317>

Hartl FU. Protein Misfolding Diseases. Annual Review of Biochemistry. 2017 Jun 20;86:21-26. doi: 10.1146/annurev-biochem-061516-044518. Epub 2017 Apr 24. PMID: 28441058

Janmey PA, Stossel TP. Modulation of gelsolin function by phosphatidylinositol 4,5-bisphosphate. *Nature*. 1987 Jan 22-28;325(6102):362-4. doi: 10.1038/325362a0. PMID: 3027569.

Johnson SM, Wiseman RL, Sekijima Y, Green NS, Adamski-Werner SL, Kelly JW. Native State Kinetic Stabilization As a Strategy To Ameliorate Protein Misfolding Diseases: A focus on the Transthyretin Amyloidoses. *Accounts of Chemical Research*. 2005;38:911–921. doi: 10.1021/ar020073i.

Kim, M. S., Pinto, S. M., Getnet, D., et al. (2014). A draft map of the human proteome. *Nature*, 509(7502), 575–581. <https://doi.org/10.1038/nature13302>

Kiuru S, Matikainen E, Kupari M, Haltia M, Palo J. Autonomic nervous system and cardiac involvement in familial amyloidosis, Finnish type (FAF). *Journal of the Neurological Sciences*. 1994; 126:40–48. [PubMed: 7836945]

Kiuru S. Gelsolin-related familial amyloidosis, Finnish type (FAF), and its variants found worldwide. *Amyloid: the Journal of Protein Folding Disorders*. 1998 Mar;5(1):55-66. doi: 10.3109/13506129809007291. PMID: 9547007.

Kiuru-Enari S, Somer H, Seppalainen AM, Notkola IL, Haltia M. Neuromuscular pathology in hereditary gelsolin amyloidosis. *Journal of Neuropathology & Experimental Neurology*. 2002; 61:565–571. [PubMed: 12071640]

S. Kiuru-Enari, J. Keski-Oja, M. Haltia, Cutis laxa in hereditary gelsolin amyloidosis, *British Journal of Dermatology*, Volume 152, Issue 2, 1 February 2005, Pages 250–257, <https://doi.org/10.1111/j.1365-2133.2004.06276.x>

Kiuru-Enari S, Haltia M. Hereditary gelsolin amyloidosis. *Handbook of Clinical Neurology*. 2013;115:659–681.

Kothakota, S., Azuma, T., Reinhard, C., Klippel, A., Tang, J., Chu, K., McGarry, T. J., Kirschner, M. W., Kohts, K., Kwiatkowski, D. J., & Williams, L. T. (1997). Caspase-3-generated fragment of gelsolin: Effector of morphological change in apoptosis. *Science*, 278(5336), 294–298. <https://doi.org/10.1126/science.278.5336.294>

M. Kramer, Chapter 6 - Intracellular Calcium, Editor(s): IJstrand M. Kramer, Signal Transduction (Third Edition), Academic Press, 2016, Pages: 381-439, ISBN: 9780123948038, <https://doi.org/10.1016/B978-0-12-394803-8.00006-1>. (<https://www.sciencedirect.com/science/article/pii/B9780123948038000061>)

Kwiatkowski, D. J., Stossel, T. P., Orkin, S. H., Mole, J. E., Colten, H. R., & Yin, H. L. (1988). Plasma and cytoplasmic gelsolins are encoded by a single gene and contain a duplicated actin-binding domain. *Nature*, 323(6087), 455–458.

<https://doi.org/10.1038/323455a0>

Lashuel HA, Hartley D, Petre BM, Walz T, Lansbury PT. Neurodegenerative disease: Amyloid pores from pathogenic mutations. *Nature*. 2002;418:291. doi: 10.1038/418291a.

Levy E, Haltia M, Fernandez-Madrid I, Koivunen O, Ghiso J, Prelli F, Frangione B. Mutation in gelsolin gene in Finnish hereditary amyloidosis. *Journal of Experimental Medicine*. 1990 Dec 1;172(6):1865-7. doi: 10.1084/jem.172.6.1865. PMID: 2175344; PMCID: PMC2188742.

Solomon JP, Page LJ, Balch WE, Kelly JW. Gelsolin amyloidosis: genetics, biochemistry, pathology and possible strategies for therapeutic intervention. *Critical Reviews in Biochemistry and Molecular Biology*. 2012 May-Jun;47(3):282-96. doi: 10.3109/10409238.2012.661401. Epub 2012 Feb 24. PMID: 22360545; PMCID: PMC3337338.

Makioka, K., Ikeda, M., Ikeda, Y., Nakasone, A., Osawa, T., Sasaki, A., ... Okamoto, K. (2010). Familial amyloid polyneuropathy (Finnish type) presenting multiple cranial nerve deficits with carpal tunnel syndrome and orthostatic hypotension. *Neurological Research*, 32(5), 472–475. <https://doi.org/10.1179/174313209X409007>

Maury, C. P. J., Kere, J., Tolvanen, R., & de la Chapelle, A. (1990). Finnish hereditary amyloidosis is caused by a single nucleotide substitution in the gelsolin gene. *FEBS Letters*, 276(1–2), 75–77

Maury CP, Baumann M. Isolation and characterization of cardiac amyloid in familial amyloid polyneuropathy type IV (Finnish): relation of the amyloid protein to variant gelsolin. *Biochimica et Biophysica Acta*. 1990 Nov 14;1096(1):84-6. doi: 10.1016/0925-4439(90)90016-i. Erratum in: *Biochim Biophys Acta* 1991 Jun 5;1096(4):361. PMID: 2176550.

Meretoja J. Familial systemic paramyloidosis with lattice dystrophy of the cornea, progressive cranial neuropathy, skin changes and various internal symptoms. A previously unrecognized heritable syndrome. *Annals of Clinical Research*. 1969; 1:314–324. [PubMed: 4313418]

Meretoja J. Genetic aspects of familial amyloidosis with corneal lattice dystrophy and cranial neuropathy. *Clinical Genetics*. 1973; 4:173–185. [PubMed: 4543600]

Mendelson L, Prokaeva T, Lau KHV, Sanchorawala V, McCausland K, Spencer B, Dasari S, McPhail ED, Kaku MC. Hereditary gelsolin amyloidosis: a rare cause of

cranial, peripheral and autonomic neuropathies linked to D187N and Y447H substitutions. *Amyloid*. 2023 Dec;30(4):357-363. doi: 10.1080/13506129.2023.2204999. Epub 2023 May 4. PMID: 37140928.

S. Nag, Q. Ma, H. Wang, S. Chumnarnsilpa, W.L. Lee, M. Larsson, B. Kannan, M. Hernandez-Valladares, L.D. Burtnick, & R.C. Robinson, Ca<sup>2+</sup> binding by domain 2 plays a critical role in the activation and stabilization of gelsolin. *Proceedings of the National Academy of Sciences of the United States of America* 106 (33) 13713-13718, <https://doi.org/10.1073/pnas.0812374106> (2009).

Olzscha H, Schermann SM, Woerner AC, Pinkert S, Hecht MH, Tartaglia GG, Vendruscolo M, Hayer-Hartl M, Hartl FU, Vabulas RM. Amyloid-like aggregates sequester numerous metastable proteins with essential cellular functions. *Cell*. 2011 Jan 7;144(1):67-78. doi: 10.1016/j.cell.2010.11.050. PMID: 21215370.

Oregel, K. Z., Shouse, G. P., Oster, C., Martinez, F., Wang, J., Rosenzweig, M., Deisch, J. K., Chen, C. S., & Nagaraj, G. (2018). Atypical presentation of gelsolin amyloidosis in a man of African descent with a novel mutation in the gelsolin gene. *American Journal of Case Reports*, 19, 374-381. <https://doi.org/10.12659/AJCR.907550>

Riordan, J. R., Rommens, J. M., Kerem, B.-S., Alon, N., Rozmahel, R., Grzelczak, Z., ... & Collins, F. S. (1989). Identification of the cystic fibrosis gene: Cloning and characterization of complementary DNA. *Science*, 245(4922), 1066–1073. <https://doi.org/10.1126/science.2475911>

Tanford, C. (1980). *The hydrophobic effect: Formation of micelles and biological membranes* (2nd ed., pp. 64–68). Wiley.

Venter, J. C., Adams, M. D., Myers, E. W., et al. (2001). The sequence of the human genome. *Science*, 291(5507), 1304–1351. <https://doi.org/10.1126/science.1058040>

Walsh DM, Klyubin I, Fadeeva JV, Cullen WK, Anwyl R, Wolfe MS, Rowan MJ, Selkoe DJ. Naturally secreted oligomers of amyloid  $\beta$  protein potently inhibit hippocampal long-term potentiation in vivo. *Nature*. 2002;416:535–539. doi: 10.1038/416535a.

Walsh DM, Selkoe DJ. A $\beta$  oligomers -a decade of discovery. *Journal of Neurochemistry*. 2007;101:1172–1184. doi: 10.1111/j.1471-4159.2006.04426.x.

Walsh MJ, Cooper-Knock J, Dodd JE, Stopford MJ, Mihaylov SR, Kirby J, Shaw PJ, Hautbergue GM. Invited review: decoding the pathophysiological mechanisms that underlie RNA dysregulation in neurodegenerative disorders: a review of the current state of the art. *Neuropathology & Applied Neurobiology*. 2015 Feb;41(2):109-34. doi: 10.1111/nan.12187. PMID: 25319671; PMCID: PMC4329338.

Wilhelm, M., Schlegl, J., Hahne, H., et al. (2014). Mass-spectrometry-based draft of the human proteome. *Nature*, 509(7502), 582–587. <https://doi.org/10.1038/nature13319>

## **CURRICULUM VITAE**

